

Skewing Technology for Permanent Magnet Synchronous Motors: A Comprehensive Review and Recent Trends

REN TSUNATA ^{ID} (Member, IEEE) AND MASATSUGU TAKEMOTO ^{ID} (Member, IEEE)

Graduate School of Environmental, Life, Natural Science and Technology, Okayama University, Okayama 700-8530, Japan

CORRESPONDING AUTHOR: REN TSUNATA (e-mail: tsunata@okayama-u.ac.jp).

ABSTRACT This article gives a comprehensive overview of the current research trends in the skewing technique for permanent magnet synchronous motors (PMSMs). The skewing technique has been widely used in many applications to reduce the cogging torque and torque ripple in PMSMs. There are many ways to implement the skew, and new techniques are continually being developed. First, this article summarizes the types of skew structures and presents a survey of existing techniques. Specific emphasis is placed on what kind of skew structure is selected depending on the PMSM configuration. Second, the optimal value of the skew angle for each structure is comprehensively explained, and the discrepancy between theory and finite element analysis is discussed. The definition of skew angle varies across the literature, and one of the purposes of this article is to organize the definition in an easy-to-understand manner. In addition, this article offers three-dimensional finite element analysis (3D-FEA) results of various PMSMs employing the skew for quantitative comparison. Then, this article discusses the properties of PMSMs using the skew by structure and the latest trends, and finally describes future prospects.

INDEX TERMS Additive manufacturing (AM), axial leakage flux, cogging torque, electrical machine, finite element analysis (FEA), induction motor (IM), interior permanent magnet synchronous motor (IPMSM), noise, patents, permanent magnet synchronous motor (PMSM), skew, surface permanent magnet synchronous motor (SPMSM), torque ripple, total harmonic distortion (THD), traction motor, transportation, vibration.

NOMENCLATURE

N	Number of research reports.	B_{am}	Coefficient related to magnetic flux density in air gap.
N_p	Number of poles.	k_w	Winding factor.
N_s	Number of slots.	k_p	Pitch factor.
M	Number of steps in step skew.	k_d	Distribution factor.
T_{cog}	Cogging torque.	k_s	Skew factor.
θ_m	Mechanical angle.	k_{sn}	Skew factor of n th component.
θ_{cog}	Angle of one cycle of cogging torque.	ψ_{pm}	Magnetic flux of permanent magnet.
θ_{skew_theo}	Theoretical skew angle.	I_m	Armature current.
θ_{skew_step}	Skew angle for each step.	β	Phase angle of armature current.
θ_{skew}	Total skew angle.	F_z	Axial force.
μ_o	Permeability of vacuum.	θ_{shift}	Stator shift angle.
L	Stack length.	θ_{slot}	Slot pitch angle.
R_1	Air gap inner radius.	δ_n	Theoretical shift angle of tooth-tips.
R_2	Air gap outer radius.	α_a	Wider pole width in asymmetric pole rotor.
G_{ak}	Coefficient related to relative permeability.	α_b	Narrower pole width in asymmetric pole rotor.

I. INTRODUCTION

Permanent magnet synchronous motors (PMSMs) are widely used in many applications due to their high efficiency [1]. However, permanent magnets (PMs) generate cogging torque, which increases vibration and noise [2]. In addition, demand for electric vehicles (EVs) has increased, and reducing torque ripple in traction motors is also important [3]. The skewing technique is frequently used to reduce the cogging torque and torque ripple in PMSMs [4]. Although skewing technology has a long history, demand for PMSMs has increased in recent years, and thus, new skewing technology is constantly being developed. Many literature works have reported on reducing torque ripple through optimizing parameters and combination of appropriate number of poles and slots [5], [6], [7]. However, optimizing parameters requires many analyses. Hence, in addition to taking a lot of time to design, it also places a heavy load on the computer. In contrast, the skew can easily reduce the cogging torque without major parameter optimization because the harmonic order of the ripple to be reduced can be theoretically calculated. Furthermore, the use of skewing technology has benefits other than reducing the torque ripple and cogging torque, and as a result, it is widely used in many applications.

Fig. 1 shows the trends in the number of contributions dedicated to skewing techniques for PMSMs or induction motors (IMs) in the IEEE Explore Digital Library. The skewing technique has been used in IMs for decades [see Fig. 1(a)], with the first paper dating back to 1928 [8]. Three-dimensional (3D) finite element analysis (FEA) is effective for verifying the effects of skewing [9]. 3D-FEA began to become popular in the 1980s, and the number of submitted papers about the skewing technique has been increasing since then. The number of papers on skewing technology for IMs has also been increasing. Fig. 1(b) shows that the number of papers dedicated to PMSMs using skewing technology has also increased since the 1980s when 3D-FEA became popular. Furthermore, because PMSMs were slower to spread than IMs, the first paper on the skew for a PMSM was published in 1983 [10]. Around the same time, rare earth PMs began to become popular [11].

With the spread of PMSMs, the number of reports on skewing technology has increased dramatically over the last two decades, and the number of reports is nearly twice that for IMs. Reports on PMSMs using a skew have included not only those about the structures but also those on analysis and manufacturing methods [12], [13].

Thus, skewing techniques for PMSMs are an important technology and are being considered by many research institutions. Various structures and theories have been reported for the skewing technology for PMSMs. In addition, skewing technology has been increasingly used for purposes other than reducing the cogging torque and torque ripple. The same can be said for patents related to the skew shown in Fig. 2, whose number has increased rapidly since the same period. The number of patents is greater than the number of academic papers, and there are many documents related to manufacturing

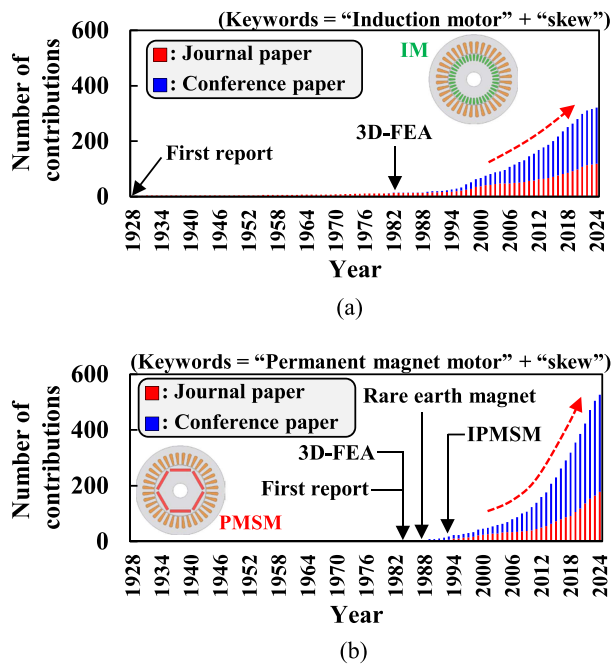


FIGURE 1. Trends in the number of contributions dedicated to IMs and PMSMs using skewing technology. (a) IMs. (b) PMSMs.

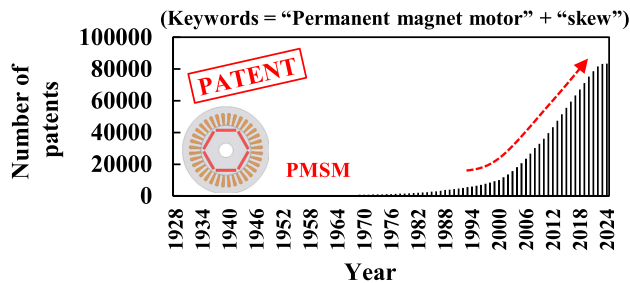


FIGURE 2. Trends in the number of patents dedicated to PMSMs using skewing technology.

methods. However, to the authors’ knowledge, there is no literature that comprehensively summarizes skewing technologies. In addition, skewing technology continues to develop due to advances in materials and manufacturing. Therefore, this article provides a comprehensive overview of skewing technology in PMSMs and a clear summary of current research trends.

This article is organized as follows. In Section II, the different types of skew structures are explained. In addition, a survey of existing skew structures is shown. Based on the survey, this article focuses on how the choice of skew structure depends on the PMSM configuration. In Section III, appropriate theoretical skew angle is accurately discussed and organized because the definition of skew angles differs depending on the article, causing confusion. In Section IV, 3D-FEA results of various PMSMs employing the skew for quantitative comparison are shown. In Section V, the properties of PMSMs using different skew structures and the current

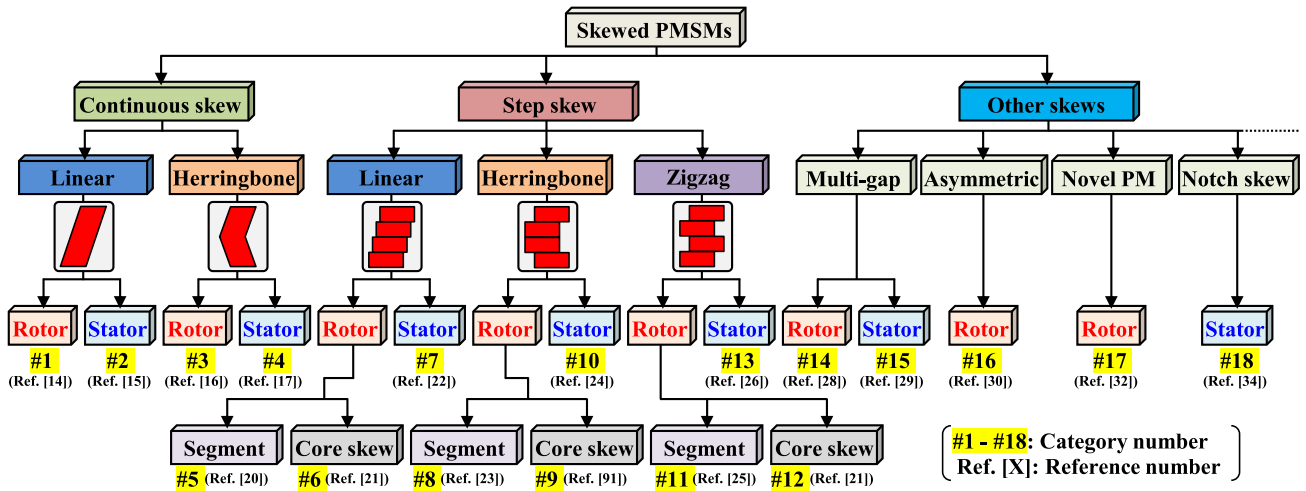


FIGURE 3. Classification of PMSMs using skewing techniques and corresponding references.

state-of-the-art for each are reviewed. This section also discusses the accuracy of FEA-predicted skew characteristics based on experimental results. In Section VI, based on the 3D-FEA results and references, advantages and disadvantages of each skew structure are discussed. Finally, the article is concluded in Section VII.

II. CLASSIFICATION OF PMSMS USING SKEW

A. CATEGORY OF PMSMS USING SKEW

This section describes the classification of structures using a skew, although the characteristics of each structure are explained in detail in Section IV. The skewing technique used depends on the PMSM structure, and Fig. 3 provides a comprehensive classification of reported skew structures. In this article, skew structures are divided into 18 categories (#1 to #18) to discuss each category. Generally, the skew is used to reducing the cogging torque and torque ripple by stacking the laminated steel sheet (LSS) in the axial direction while shifting LSS in the direction of rotation. First, skew structures can be roughly divided into continuous skews (#1 to #4) and step skews (#5 to #13) depending on the stacking method. In addition, we refer to skew structures that do not fall into these categories as other skews (#14 to #18).

In the continuous skew structure, the layers are stacked and shifted continuously in the axial direction so that angular displacement in the rotational direction is smooth. This structure can be classified further depending on the lamination method as a linear or herringbone skew. In the linear skew structure, the layers are laminated with angular displacement in only one direction and it is a typical skew (#1 [14], #2 [15]). In the herringbone skew structure, the direction of angular displacement changes midway through (#3 [16], #4 [17]). The herringbone skew is also called a V-shaped skew because its position changes in the axial direction like a V-shape [18]. Both structures can be classified further depending on whether the skew is in the rotor or the stator. Although the continuous skew structure is highly effective in suppressing problems

such as cogging torque, it generally has poor manufacturability because it requires continuous angular displacement and lamination.

In the step skew structure, rotor or stator is divided by the number of steps M in the axial direction and is stacked with a shift in the rotational direction. Because there is no displacement in the rotational direction within each step, the step skew structure is excellent in terms of manufacturability [19]. Step skew structures can be classified into three types based on the lamination pattern of each step. Similar to the continuous skew structure, a structure in which the direction of displacement is only in one direction is called a linear skew (#5 to #7) [20], [21], [22], and a structure in which the direction of displacement changes to the opposite direction halfway through is called a herringbone skew (#8 to #10) [21], [23], [24]. Furthermore, a structure in which the displacement direction of each step alternates is called a zigzag skew (#11 to #13) [21], [25], [26]. The three structures using step skew can be classified further into two patterns based on the pattern in which the rotor is skewed. Generally, a PMSM rotor is composed of PMs and LSS. Segment patterns (#5 [20], #8 [23], and #11 [25]) have a structure that displaces both the PM and the LSS. In contrast, core skew patterns (#6, #9, and #12) have a structure that does not displace the PM and only the shape of the LSS is changed [21]. Furthermore, when introducing the step skew in the stator, the core skew structure is most often adopted from the viewpoint of winding installation [22], [24], [27].

The multigap skew is in the other skew structure category. This structure can be used when there are two stators or rotors, that is, when there are multiple air gaps. For example, for a double rotor structure, the cogging torque can be reduced by shifting the mutual positions of the rotors (#14 [28]). Similarly, for a double stator structure, the same effect as a skew can be obtained by shifting the positional relationship of the two stators (#15 [29]). An asymmetric skew has a structure in which, for example, the shape of the PM or core differs

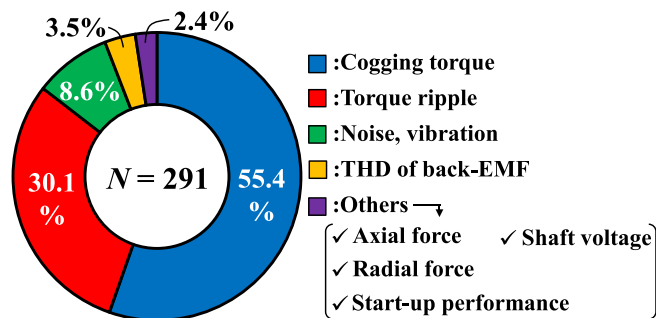


FIGURE 4. Purpose of the skew in PMSMs [number of survey reports $N = 291$ from data on journal papers and conference papers from 2014 to 2024 in Fig. 1(b)].

between the N and S poles (#16 [30], [31]). Because there is no angular displacement in the rotational direction, it can be assembled in the same way as for typical PMSMs. There are also structures that achieve skew effects using special PM structures (#17 [32]). By using PMs with different shapes in the axial direction, the locations where the cogging torque is generated can be dispersed. One method for suppressing the cogging torque and torque ripple is to include a notch at the tooth tip of the stator core [33]. There are also structures in which this notch is displaced in the rotational direction like a skew (#18 [34]).

There are many skewing techniques, and it is necessary to select an appropriate technique for the purpose, manufacturability, and material used. New skew structures may be developed based on future advances in manufacturing technology and materials.

B. SURVEY OF PURPOSES OF SKEWING TECHNOLOGIES IN PMSMS

Fig. 4 shows the proportion of the skew for each purpose in PMSMs. The number of research reports is $N = 291$ (IEEE Explore Digital Library). The main purpose of the skew in PMSMs to reduce cogging torque and torque ripple accounts for 55.4% and 30.1% of reports, respectively. The skew is also used to reduce the vibration and noise [35], [36], and to suppress the total harmonic distortion (THD) of the back electromotive force (EMF) of PMSMs [37]. The use of a skew to reduce the axial and radial forces to reduce the load on the bearings has been examined [38], [39]. The skew is also effective in improving the starting characteristics of line-start PMSMs and suppressing shaft voltage [40], [41].

Fig. 5 shows the proportion of usage by skew structure. Fig. 5(a) shows a breakdown of the continuous skew and the step skew when the rotor is skewed. In addition, we also separate surface permanent magnet synchronous motors (SPMSMs) and interior permanent magnet synchronous motors (IPMSMs). The proportions of SPMSMs and IPMSMs using the step skew are high at 40.6% and 36.8%, respectively. The continuous skew is rarely used for rotors. In particular, for IPMSMs, if the continuous skew is used, it is difficult to insert

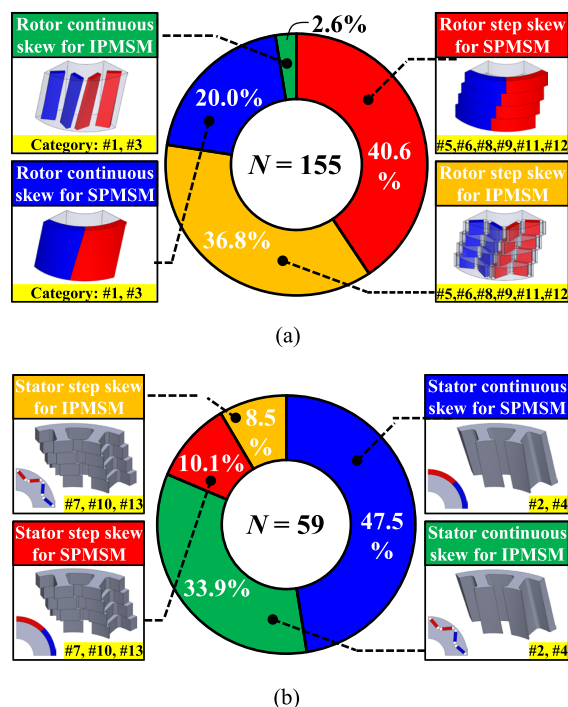


FIGURE 5. Usage percentage by skew category from data on journal papers and conference papers from 2014 to 2024 in Fig. 1(b). (a) Rotor configuration ($N = 155$). (b) Stator configuration ($N = 59$).

PMs into the LSSs, and the manufacturability is extremely poor [42]. Consequently, the proportion of IPMSMs using the continuous skew for the rotor is only 8.5%. SPMSMs are used more often than IPMSMs because they have PMs on the outside of the rotor and can achieve the continuous skew through dedicated magnetization [43], [44].

Fig. 5(b) shows a breakdown of the continuous skew and the step skew when a skew is provided in the stator. For stators, the trend is opposite to that of rotors, and the proportion of continuous skew use is high for both IPMSMs and SPMSMs. The proportions of SPMSMs and IPMSMs with a step skew in the stator are only 10.1% and 8.5%, respectively, which is because dead space occurs between the stator core and the windings, and the coil space factor decreases. The numbers of reports of use of rotor skews and stator skews are $N = 155$ and 59, respectively, which suggests that rotor skews are more widely used. The percentages of rotor and stator skews in Fig. 5(a) and (b), respectively, are higher in SPMSMs because although IPMSMs can reduce the cogging torque by changing the shape of the rotor core, it is difficult to do so with SPMSMs owing to the PM being on the surface [45].

C. MARKET PRODUCT USING SKEW

Skewing technology is also widely used in PMSMs in the industrial sector. In particular, traction motors for EVs and hybrid electric vehicles (HEVs) require low torque ripples to ensure driving comfort. Cogging torque and torque ripple can

TABLE 1 Skew Type of Traction Motors (PMSM) Mounted on Commercially Supplied EVs and HEVs

	ID.3 (Volks wagen)	Model3 (Tesla)	IONIQ5 (Hyundai)	F-150 Lightning (Ford)	LEAF (Nissan)	Prius 4 th (Toyota)	FREED (Honda)
Vehicle type	EV	EV	EV	EV	EV	HEV	HEV
Skew type	Step skew (rotor)	Step skew (rotor)	Step skew (rotor)	Step skew (rotor)	Step skew (rotor)	Un- skewed	Un- skewed
	Linear	Herring- bone	Zigzag	Herring- bone	Linear		
No. of steps M	$M = 4$	$M = 3$	$M = 4$	$M = 8$	$M = 2$		
Category No.	#5	#8	#11	#8	#5		

be suppressed by appropriately selecting the combination of the number of poles and slots [46], [47]. However, the skew is generally used because it is difficult to completely eliminate the cogging torque and torque ripple by only selecting the combination of the number of poles and slots.

Table 1 summarizes the skew type used in traction motors for commercially supplied EVs and HEVs. EVs do not have the engine, and hence, characteristics of the traction motor are directly linked to driving performance. Accordingly, traction motors for EVs basically employ the skew. In addition, the large stack length of EV traction motors also makes it easier to employ the skew. These traction motors for EVs employ the step skew but various categories are chosen. When the main focus is on reducing the torque ripple and cogging torque, the linear step skew (#5) is often used. However, when the number of steps M is large, the manufacturing cost increases. Hence, in some cases, the number of steps M may be reduced to prioritize cost. On the other hand, the linear skew (#5) generates axial electromagnetic force, which can cause problems with bearing loss, noise, and lifespan. Therefore, the herringbone skew (#8) or zigzag skew (#11) may be used to suppress the axial electromagnetic force. The quantitative differences between each category are explained in detail in the comparison using 3D-FEA in Section IV.

Fig. 6 shows the photographs of some rotors obtained by disassembling commercially available traction motors. Fig. 6(a) shows the rotor of traction motor installed in IONIQ5, which uses category #11 with $M = 4$. A traction motor of Nissan Leaf shown in Fig. 6(b) uses category #5 with $M = 2$ and is designed to cancel only the fundamental component of the cogging torque. Furthermore, Fig. 6(c) shows the rotor of an IM for the rear-wheel drive of Toyota Prius 4th generation, which has the continuous skew of category #1. In the case of IMs, it is relatively easy to employ the continuous skew to the rotor because they are molded as a single unit using the aluminum die casting [48].

III. THEORY OF SKEWING TECHNIQUE AND SKEW ANGLE

A. COGGING TORQUE

This section describes the theory of the skewing technique, focusing on the skew angle. Many research groups have

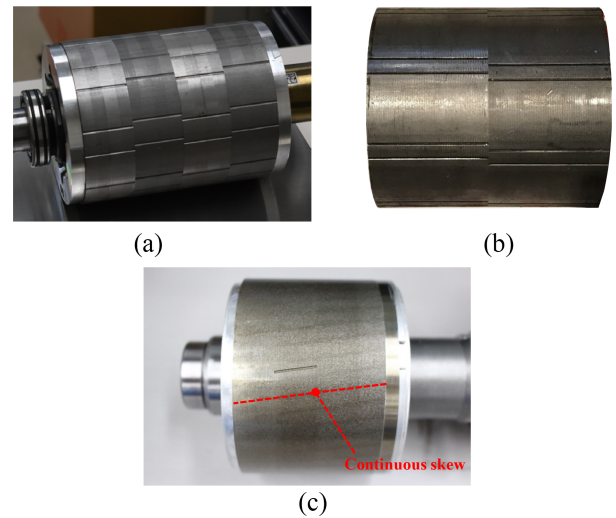


FIGURE 6. Rotor photographs of traction motors using skew in commercially supplied EVs and HEVs. (a) Category #11 rotor of Hyundai IONIQ5. (b) Category #5 rotor of Nissan LEAF. (c) Category #1 rotor of Toyota Prius 4th (IM for rear-wheel drive).

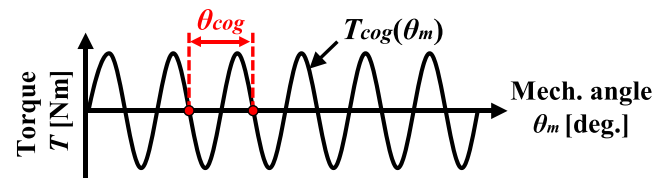


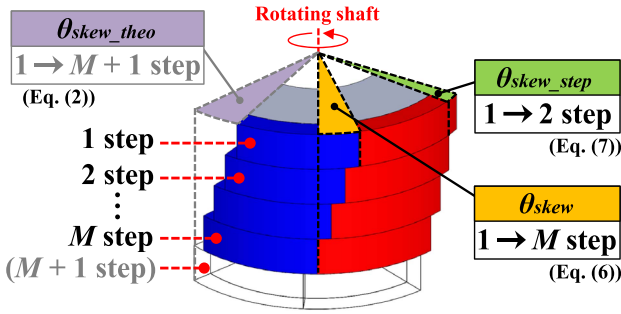
FIGURE 7. Example of cogging torque waveform for a PMSM.

performed theoretical studies to minimize the cogging torque and torque ripple. However, the definition of skew angle varies across the literature, which can lead to confusion, and one of the purposes of this article is to organize the definition in an easy-to-understand manner. In addition, the relationship between the skew factor k_s and torque is also explained.

To suppress the cogging torque theoretically, it is necessary to express it mathematically. Fig. 7 shows an example of the cogging torque waveform. First, the angle θ_{cog} of one cycle of the cogging torque can be expressed as follows [49], [50], [51]:

$$\theta_{cog} = \frac{360^\circ}{\text{LCM}(N_p, N_s)}. \quad (1)$$

Here, N_p and N_s are the number of poles and slots in the PMSM, respectively. $\text{LCM}(N_p, N_s)$ is the least common multiple of N_p and N_s . Therefore, the cogging torque period depends on the number of poles and the number of slots, and the larger the $\text{LCM}(N_p, N_s)$, the shorter the period. Consequently, the larger the $\text{LCM}(N_p, N_s)$, the smaller the amplitude of the cogging torque tends to be [52], [53]. In addition, Nian et al. [54] showed a theoretical skew angle θ_{skew_theo} that can theoretically minimize the cogging torque in a PMSM with an arbitrary number of poles and slots. θ_{skew_theo} can be


FIGURE 8. Step skewing scheme for a PMSM with number of steps M .

expressed as follows:

$$\theta_{skew_theo} = \theta_{cog} = \frac{360^\circ \times \text{GCD}(N_p, N_s)}{N_p N_s}. \quad (2)$$

Here, $\text{GCD}(N_p, N_s)$ is the greatest common divisor of N_p and N_s . Furthermore, θ_{skew_theo} is equal to θ_{cog} when N_p and N_s are integers. Therefore, the theoretical skew angle determined only by the number of poles and the number of slots is period θ_{cog} of the cogging torque.

When using a step skew, it is necessary to consider the number of steps M and select an appropriate skew angle. Therefore, Nian et al. [54] derived optimal skew angle θ_{skew} considering M . Fig. 8 shows a schematic of a PMSM using a step skew with M steps, showing that θ_{skew} is the total skew angle. First, cogging torque $T_{cog}(\theta_m)$ shown in Fig. 7 is formulated as follows without considering the skew:

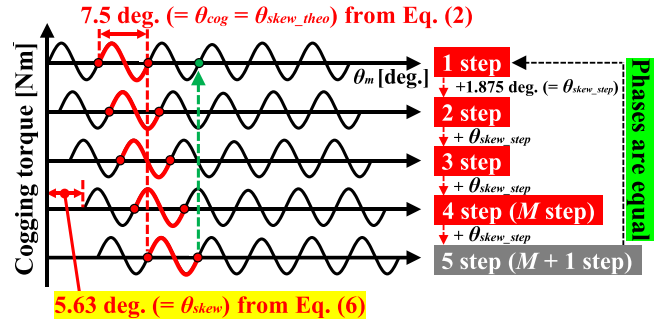
$$T(\theta_m) = \frac{\pi L \times \text{LCM}(N_p, N_s)}{4\mu_o} (R_2^2 - R_1^2) \times \sum_{n=1}^{\infty} n G_{ak} B_{am} \sin(n\theta_m \times \text{LCM}(N_p, N_s)). \quad (3)$$

Here, L is the stack length. R_1 and R_2 are the air gap of inner and outer radiuses, respectively. G_{ak} and B_{am} are coefficients related to the relative permeability and the magnetic flux density of air gap, respectively. Equation (3) can be written as follows considering skew [54]:

$$T(\theta_m) = \frac{\pi L \times \text{LCM}(N_p, N_s)}{4\mu_o M} (R_2^2 - R_1^2) \times \sum_{n=1}^{\infty} n G_{ak} B_{am} \frac{\sin \frac{n\theta_{skew} \times \text{LCM}(N_p, N_s)}{2} \frac{M}{M-1}}{\sin \frac{n\theta_{skew_step} \times \text{LCM}(N_p, N_s)}{2}} \times \sin \left[n \left(\theta_m + \frac{\theta_{skew_step}}{2} \right) \times \text{LCM}(N_p, N_s) \right]. \quad (4)$$

Here, θ_{skew_step} is the skew angle for each step. To reduce the cogging torque, it is sufficient that $T_{cog} = 0$ in (4). To satisfy $T_{cog} = 0$, the following equation must hold true:

$$\sin \frac{n\theta_{skew} \times \text{LCM}(N_p, N_s)}{2} \frac{M}{M-1}. \quad (5)$$


FIGURE 9. Cogging torque waveforms for each step in an example with $N_p = 8$, $N_s = 48$, and $M = 4$.

θ_{skew} that satisfies (5) can be expressed as

$$\theta_{skew} = \frac{M-1}{M} \times \frac{360^\circ}{\text{LCM}(N_p, N_s)}. \quad (6)$$

The optimal skew angle for PMSM with M steps can be calculated using (6). In addition, the skew angle for each step θ_{skew_step} is calculated as follows [55]:

$$\theta_{skew_step} = \frac{\theta_{skew}}{M-1}. \quad (7)$$

θ_{skew_theo} and θ_{skew} are different (see Fig. 8), and θ_{skew_theo} in (2) corresponds to the total skew angle up to the virtual $(M+1)$ th step. Fig. 9 shows an example of the cogging torque waveform for each step when $N_p = 8$, $N_s = 48$, and $M = 4$. PMSMs using the combination of $N_p = 8$ and $N_s = 48$ are often used in EV traction motors [56], [57], [58]. According to (6), the appropriate total skew angle θ_{skew} is 5.625°. From (7), skew angle θ_{skew_step} of each step is 1.875°; thus, the cogging torque waveform of each step is shifted by 1.875°. At the $(M+1)$ th position, the total skew angle becomes equal to θ_{skew_theo} obtained by (2). However, the cogging torque waveform of the $(M+1)$ th step has the same phase as the first step, so no cogging torque reduction effect can be expected. Therefore, the $(M+1)$ th step is unnecessary, and θ_{skew} is less than θ_{skew_theo} .

We plotted (2) and (6) with respect to the skew angle, as shown in Fig. 10 for the combination $N_p = 8$ and $N_s = 48$. θ_{skew_theo} calculated using (2) does not consider M , so it is constant at 7.5°. Furthermore, θ_{skew} calculated using (6) increases as M increases. In Fig. 9, the asymptote of θ_{skew} becomes θ_{skew_theo} (=7.5°). Therefore, as M increases, the appropriate skew angle approaches θ_{skew_theo} . When $M = 2$, the skew angle is half the value (3.75°) of slot angle θ_{slot} . Based on these results, θ_{skew_theo} , θ_{skew} , and θ_{skew_step} can be expressed by the following relationship:

$$\theta_{skew_theo} = \theta_{skew} + \theta_{skew_step}. \quad (8)$$

When a continuous skew is used, it can be assumed that M is large, so $\theta_{skew} \approx \theta_{skew_theo}$.

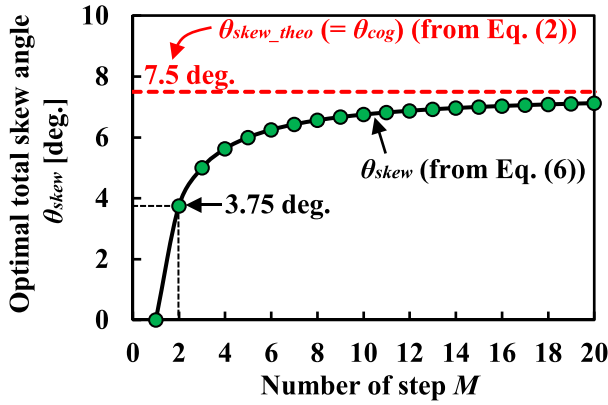


FIGURE 10. Optimal skew angle versus number of steps M (example for $N_p = 8$ and $N_s = 48$).

B. SKEW FACTOR

One of the important parameters related to PMSMs is the winding factor k_w , which is equivalent to the effectively usable magnetic flux and is therefore related to the torque characteristics. The winding factor k_w is composed of the following three factors [59]:

$$k_w = k_p k_d k_s. \quad (9)$$

Here, k_p , k_d , and k_s are the pitch factor, distribution factor, and skew factor, respectively. The pitch factor and distribution factor are values that are mainly determined by the relationship between the number of poles and slots. The skew factor k_s depends on the skew angle θ_{skew} and can be expressed by the following formula:

$$k_s = \frac{\left| \sin \frac{\theta_{skew}}{2} \right|}{\frac{\theta_{skew}}{2}}. \quad (10)$$

In addition, the skew factor k_{sn} of the n th component can also be expressed by a formula as follows [60]:

$$k_{sn} = \frac{\left| \sin \frac{n\theta_{skew}}{2} \right|}{\frac{n\theta_{skew}}{2}}. \quad (11)$$

Fig. 11 shows the skew factors k_s and k_{sn} calculated using (10) and (11). Fig. 11(a) shows the skew factor k_s of the fundamental torque, and it can be seen that as the skew angle θ_{skew} increases, the amount of magnetic flux decreases. When θ_{skew} is 360° , k_s becomes 0 and the fundamental torque is not generated. Fig. 11(b) shows the cases of $n = 36$ and $n = 48$. This is equivalent to the least common multiple LCM(N_p , N_s) of the number of poles and slots being 36 and 48, respectively. The skew angle θ_{skew} at which the skew factor k_{sn} becomes 0 differs depending on the order. When n is 48, $k_{sn} = 0$ at $\theta_{skew} = 7.5^\circ$, and hence, the theoretical skew angle θ_{skew_theo} of an 8-pole/48-slot motor is 7.5° . The exception is when $\theta_{skew} = 0^\circ$, in which case both k_s and k_{sn} are 1 because there is no skew effect.

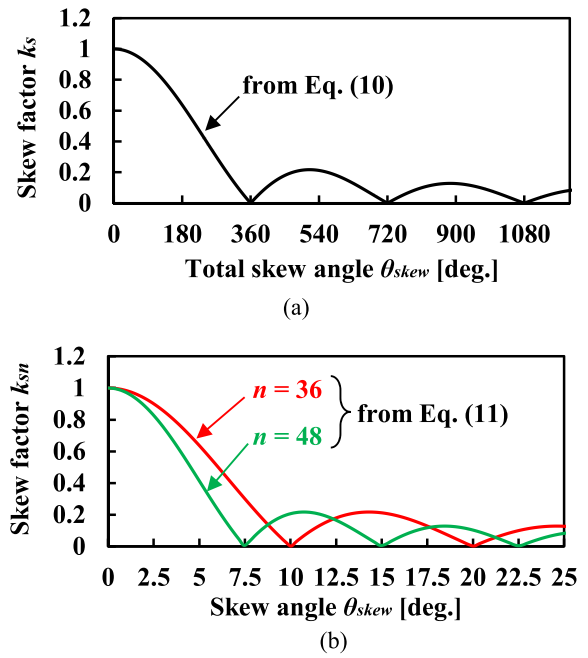


FIGURE 11. Skew factor versus skew angle (the unit of horizontal axis is [degree]). (a) Fundamental skew factor k_s . (b) Skew factor of n th components k_{sn} ($n = 36, 48$).

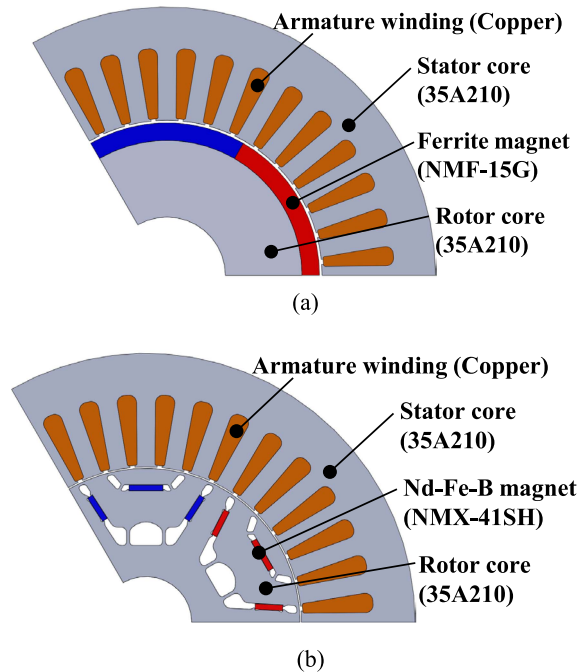


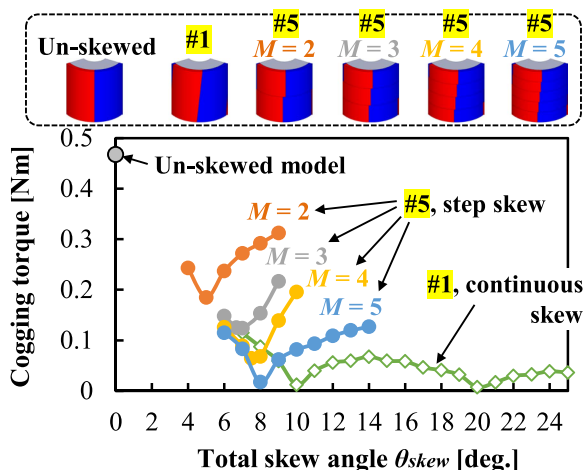
FIGURE 12. Cross-sectional views of investigated models for 3D-FEA. (a) SPMSM. (b) IPMSM.

IV. PROPERTY COMPARISON OF EACH SKEW STRUCTURE USING 3D-FEA

In this section, the authors use 3D-FEA to evaluate structures using various skews in the SPMSM and IPMSM shown in Fig. 12 and perform a quantitative comparison. Table 2 lists the parameters of the SPMSM and IPMSM, both of

TABLE 2 Parameters of SPMSM and IPMSM for Investigation

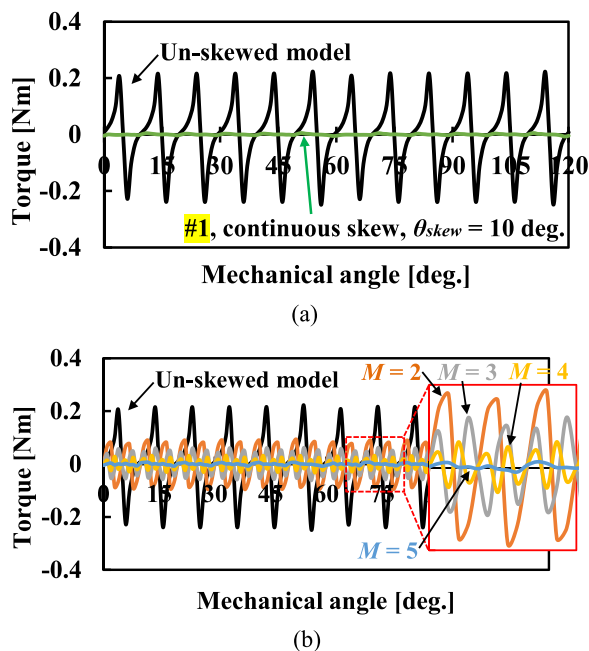
	SPMSM	IPMSM
No. of poles/slots	6p/36s	6p/36s
Winding type	Distributed winding	Distributed winding
PM material	Ferrite	Nd-Fe-B
Air gap length	0.7 mm	0.4 mm
Stack length	75 mm	75 mm
Outer diameter	147.2 mm	147.2 mm
Max. speed	7200 rpm	7200 rpm
Max. current	10 Arms	10 Arms
Rated torque	4.0 Nm	4.0 Nm


FIGURE 13. Cogging torque of SPMSM versus total skew angle in skew categories #1 and #5.

which have a 6-pole and 36-slot distributed winding structure. The SPMSM uses a ferrite magnet, and the IPMSM uses a neodymium sintered magnet, with a rated torque of 4.0 N·m. The maximum current and maximum rotation speed are 10 A_{rms} and 7200 r/min, respectively.

A. COMPARISON BETWEEN CONTINUOUS SKEW (#1) AND STEP SKEW (#5) FOR ROTOR OF SPMSM

First, this article compared the linear continuous skew (#1) and step skew (#5) that are often used in SPMSMs using 3D-FEA. Fig. 13 shows the change in the cogging torque under no-load condition when the total skew angle θ_{skew} is changed in the continuous skew model (#1) and the step skew model (#5). For comparison, the cogging torque of the unskewed model is also plotted in Fig. 13. In the step skew, the number of steps M is evaluated from 2 to 5. For each number of steps M , the skew angle θ_{skew} at which the cogging torque is minimized is different. As the number of steps M increases, the optimal skew angle θ_{skew} increases, and the effect of reducing the cogging torque also increases. This is because the larger the number of steps M can reduce various frequency components of the cogging torque.


FIGURE 14. Cogging torque waveforms of each skew model and the unskewed model. (a) Unskewed and #1 models. (b) Unskewed and #5 models.

On the other hand, the continuous skew is equivalent to a case where the number of steps M is extremely large in the step skew. As a result, the effect of reducing the cogging torque of the continuous skew is the greatest. In addition, the optimum skew angle θ_{skew} is also the largest at 10°. However, even in the step skew, when the step number M is increased to 5, it is possible to reduce the cogging torque to the same extent as in the continuous skew.

Fig. 14 compares the cogging torque waveforms of each skew model and the unskewed model. Fig. 14(a) shows the waveform of the continuous skew ($\theta_{skew} = 10^\circ$) where the cogging torque is minimized, and the cogging torque can be reduced by 97.4%. Fig. 14(b) shows the cogging torque waveform of the step skew model that employs the optimal skew angle for each step number M . As the step number M increases, the effect of reducing the cogging torque increases.

Fig. 15 shows the magnetic flux of PMs ψ_{pm} at no load versus the skew angle θ_{skew} for the continuous skew and step skew models. As the skew angle θ_{skew} increases, the skew factor k_s decreases, resulting in a decrease in the magnetic flux ψ_{pm} . In the step skew models, the smaller the number of steps M , the greater the reduction in magnetic flux. This is because when the number of steps M is small, the step skew angle θ_{skew_step} increases, resulting in large axial leakage flux between steps. In addition, the continuous skew model can reduce the axial leakage flux. As a result, the reduction in magnetic flux per skew angle θ_{skew} is smaller than the step skew models. Fig. 16 shows the average torque of each model versus the skew angle θ_{skew} when the rated current of 10 A_{rms} is applied. The current phase angle β is 0° because the SPMSM generates only the magnet torque [61]. When the

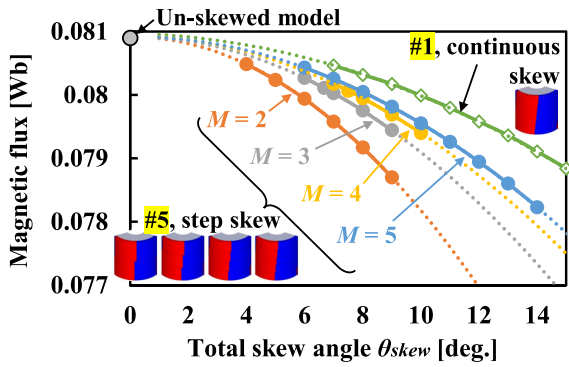


FIGURE 15. No-load magnetic flux of PMs versus total skew angle in skew categories #1 and #5.

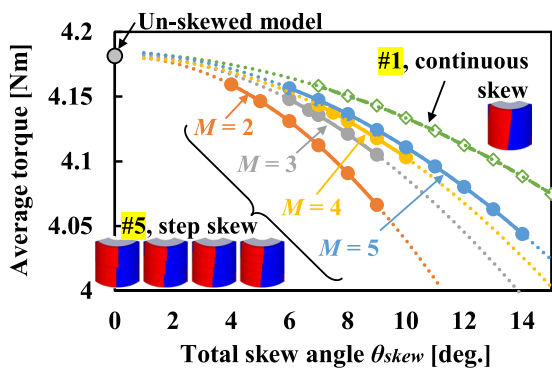
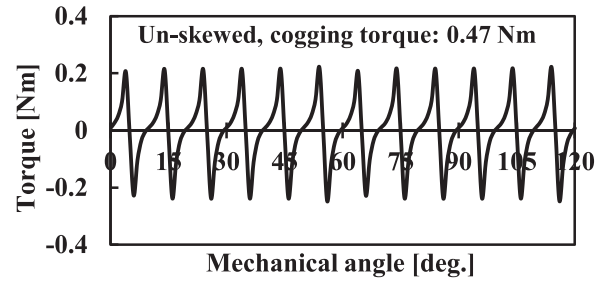


FIGURE 16. Average torque of each model versus total skew angle when the rated current of 10 A_{rms} is applied.

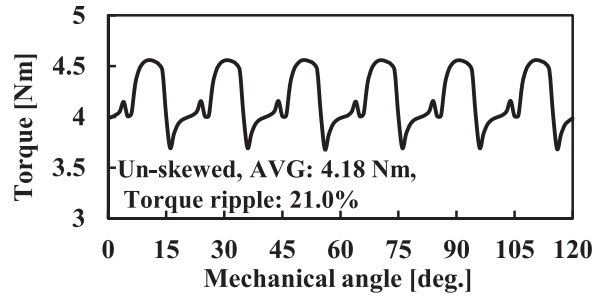
magnetic saturation does not occur, the torque of the SPMSM is proportional to the magnetic flux of PMs ψ_{pm} . Hence, the magnitude of the average torque matches the relationship in Fig. 15.

B. DIFFERENCE IN EFFECTS OF SKEW ON COGGING TORQUE AND TORQUE RIPPLE

The difference in the effect of the skew on the cogging torque and torque ripple is discussed using 3D-FEA results. Fig. 17 shows an on-load torque with 10 A_{rms} and the cogging torque waveforms of the unskewed SPMSM. The torque waveform changes significantly from that when there is no-load by applying an armature current. As a result, the spectra of each torque waveform shown in Fig. 18 also differ significantly. Fig. 18(a) shows frequency components of the cogging torque, with the 12th-order component being the largest. This is due to the slot harmonics. On the other hand, Fig. 18(b) shows frequency components of the on-load torque when the rated current is applied, with the sixth-order component, which was not present in the cogging torque, occurring and being the largest. This is due to the superposition of the magnetic flux generated by the armature winding. Therefore, it is expected that the optimal skew angle θ_{skew} will change according to

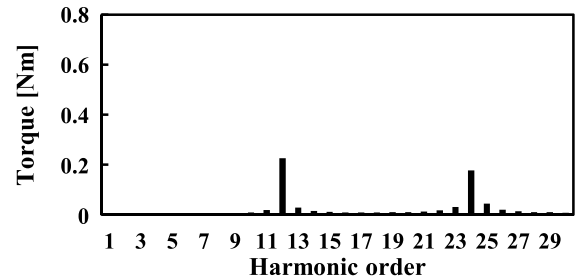


(a)

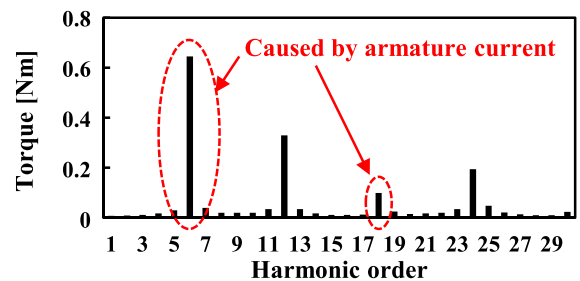


(b)

FIGURE 17. Torque waveforms of unskewed SPMSM. (a) Cogging torque. (b) On-load torque (10 A_{rms}).



(a)



(b)

FIGURE 18. Spectra of torque waveforms of unskewed SPMSM. (a) Cogging torque. (b) On-load torque (10 A_{rms}).

(11) because the frequency components of the torque waveforms were changed.

Fig. 19 shows the change in the torque ripple under on-load condition with 10 A_{rms} when the total skew angle θ_{skew} is changed in the continuous skew model (#1) and the step skew model (#5). In the step skew models (#5), as with the

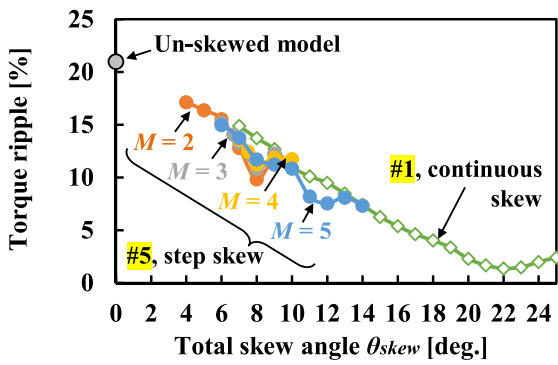


FIGURE 19. Torque ripple of SPMSM versus total skew angle in skew categories #1 and #5.

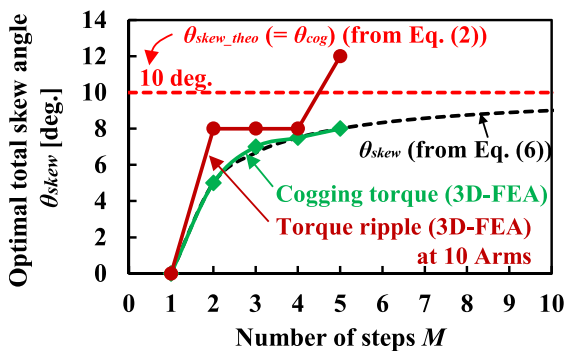


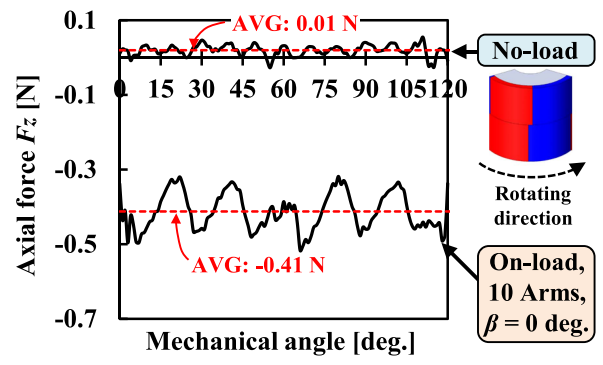
FIGURE 20. Comparison between theoretical skew angle $\theta_{skew,theo}$ calculated by equations and optimal skew angle θ_{skew} obtained by 3D-FEA for each number of steps M in SPMSM.

cogging torque, the torque ripple reduction effect increases as the number of steps M increases. In addition, the torque ripple of the continuous skew model (#1) is the lowest, and the skew angle θ_{skew} in that case is 22° . Therefore, it is significantly different from the skew angle θ_{skew} at which the cogging torque is minimum. This is because the cogging torque and the frequency components of the on-load torque are different, as shown in Fig. 18.

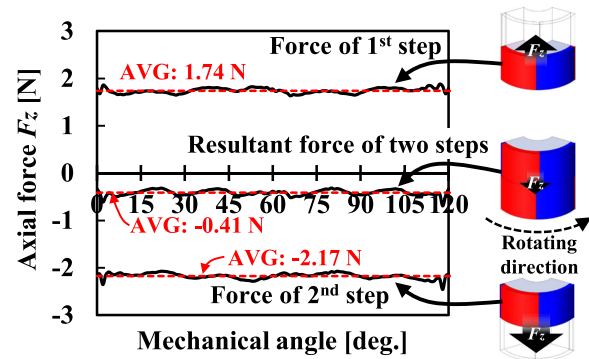
Fig. 20 compares the theoretical skew angle $\theta_{skew,theo}$ and the skew angle θ_{skew} for each number of steps M obtained by (2) and (6) with the skew angle at which the cogging torque and torque ripple of the SPMSM are minimum by 3D-FEA. It can be seen that the 3D-FEA result of the cogging torque is consistent with the skew angle obtained by (6). In contrast, for the torque ripple, there is a large error with the skew angle in (6). Therefore, when the armature current is applied, the frequency of the torque waveform may change, and the appropriate skew angle would change.

C. AXIAL FORCE CAUSED BY SKEW

It is known that the use of a skew structure causes an imbalance of magnetic flux in the axial direction, which generates an axial electromagnetic force F_z [17], [64]. In this article, the mechanism of the axial electromagnetic force generation



(a)



(b)

FIGURE 21. Axial force F_z in SPMSM using step skew with $M = 2$ and $\theta_{skew} = 5^\circ$. (a) Comparison between no-load and on-load (10 A_{rms}). (b) Comparison between each step and resultant force.

is explained using 3D-FEA results. As an example, we use a linear step skew (#5) model with $M = 2$ and $\theta_{skew} = 5^\circ$. Fig. 21 shows the analysis results of the axial electromagnetic force by 3D-FEA. Fig. 21(a) compares the axial force F_z of the entire rotor under no-load and on-load (10 A_{rms}) conditions, respectively. Under no-load condition, almost no axial force is generated, but under on-load condition, -0.41 N is generated. This axial force applies a load to the bearing, causing problems such as increased the noise and mechanical loss and reduced bearing life.

Fig. 21(b) shows results of axial electromagnetic force of each step. The axial force F_z in the first step is $+1.74$ N and occurs in the upward direction. In contrast, the axial force F_z in the second step is -2.17 N and occurs in the downward direction, which is greater than the force generated in the first step. As a result, the axial force F_z of the entire rotor is -0.41 N and acts in the downward direction.

Fig. 22 shows the magnetic flux vector diagram that shows the cause of the difference in the axial force between the first and second steps. In this model, $\theta_{skew} = 5^\circ$ and the number of poles N_p is 6, and therefore, the phase difference between the magnetic flux in the first and second steps is 15° in the electrical angle. Accordingly, as shown in Fig. 22(a), the magnetic flux of PM ψ_{pm1} in the first step leads 7.5° from the d -axis, which is the magnetic center. By applying the armature current I_m on the q -axis, the magnetic flux due to the

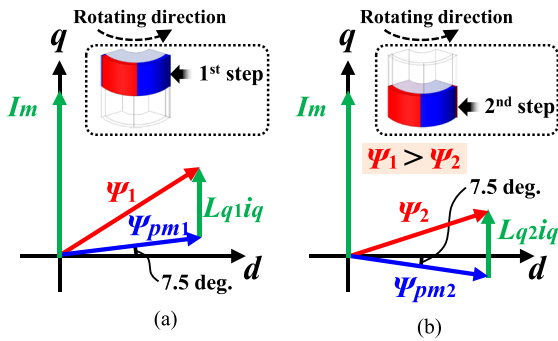


FIGURE 22. Magnetic flux vector diagram of each step in SPMSM using step skew with $M = 2$ and $\theta_{skew} = 5^\circ$ when applying load current. (a) First step. (b) Second step.

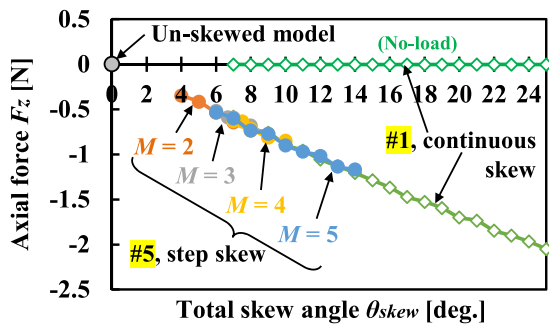


FIGURE 23. Axial force F_z of SPMSM versus total skew angle in skew categories #1 and #5.

armature current is added, and the final resultant magnetic flux in the first step becomes Ψ_1 . In contrast, the magnetic flux of PM ψ_{pm2} in the second step shown in Fig. 22(b) lags 7.5° with respect to the d -axis. The magnitude of the magnetic flux due to the armature current is the same, but because Ψ_{pm2} lags, the resultant magnetic flux ψ_2 in the second step is smaller than Ψ_1 . As a result, under on-load condition, the amount of magnetic flux generated in each step differs, and axial forces of different magnitudes are generated. In addition, when the rotor rotation direction is reversed, the direction of the axial force is also reversed.

Fig. 23 shows the change in axial force F_z versus skew angle θ_{skew} for the linear continuous skew (#1) and the linear step skew (#5) models. In all models, as the skew angle θ_{skew} increases, the difference in magnetic flux between steps increases, and therefore, the axial force F_z increases. There is almost no difference in the number of steps M , but the larger the number of steps M , the larger the optimal skew angle θ_{skew} , and hence the axial force F_z is thought to increase. In the continuous skew model, the axial force F_z under no-load condition is also shown, but it is zero regardless of the skew angle θ_{skew} .

Fig. 24 shows 3D-FEA results of the axial force F_z for the zigzag step skew (#11) having different number of steps M . In the zigzag skew, when the step number M is odd, the axial force F_z can be suppressed because it is axially symmetric.

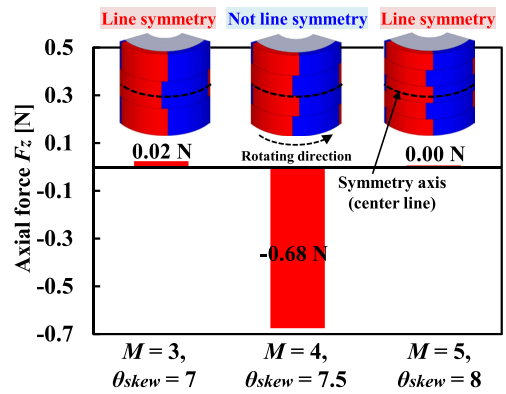


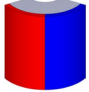
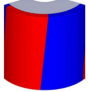
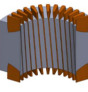
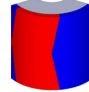
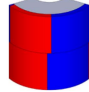
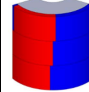
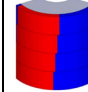
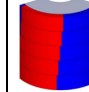
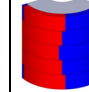
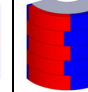
FIGURE 24. Influence of the number of steps M in zigzag skews on axial force F_z .

On the other hand, when the step number M is even, the skew model is not axially symmetric, and therefore, axial force F_z is generated. However, when the step number M is even, there is an advantage that characteristics other than the direction of the axial force do not change depending on the direction of rotation. Consequently, the zigzag skew (#11) and herringbone skew (#8) have the advantage of being able to suppress the axial force F_z under the on-load condition.

D. COMPREHENSIVE COMPARISON OF EACH SKEW

In this section, skew structures commonly used in SPMSMs are compared by 3D-FEA. Table 3 compares 3D-FEA results of each skew model. The 3D-FEA results for each model are summarized for no-load and on-load conditions. The linear continuous skew (#1) model has the highest cogging torque reduction effect, which can reduce it by 97.4% compared to the unskewed model. The herringbone continuous skew (#3) also has a small cogging torque. The continuous skew is equivalent to the step skew with an extremely large step number M , and hence it can effectively reduce the cogging torque. In addition, the linear step skew (#5) can also reduce the cogging torque very much by increasing the step number M to 5. In contrast, in the case of the herringbone step skew (#8) and zigzag step skew (#11) with the same step number $M = 5$ and $\theta_{skew} = 8^\circ$, the cogging torque is about ten times larger than that of the linear step skew (#5). This is because the step skew angle θ_{skew_step} of some steps in the herringbone skew and zigzag skew are the same and θ_{skew_step} is large. In both cases, in order to obtain the same cogging torque reduction effect as the linear step skew, the skew angle θ_{skew_step} of each step must be determined by trial and error. In addition, the step skew angle θ_{skew_step} of the herringbone step skew (#8) and the zigzag step skew (#11) is large. Accordingly, the PM magnetic flux ψ_{pm} is also greatly reduced, and the torque is reduced. However, these skew structures have the advantage of being easy to manufacture and can effectively reduce the axial force F_z . On the other hand, regarding the THD of the induced voltage, the skew structure given in Table 3 is not the optimal structure for THD because the skew angle θ_{skew}

TABLE 3 Summary of 3D-FEA Results of SPMSM Using Various Skew Structures

Specification	Category (Fig. 2)	Un-skewed	#1	#2	#3	#5 (Rotor step skew, linear)				#8	#11
	No. of steps M	-	-	-	-	$M = 2$	$M = 3$	$M = 4$	$M = 5$	$M = 5$	$M = 5$
	Appearance										
	Total skew angle θ_{skew}	-	10 deg. (optimal)	10 deg. (optimal)	10 deg. (optimal)	5 deg. (optimal)	7 deg. (optimal)	7.5 deg. (optimal)	8 deg. (optimal)	8 deg.	8 deg.
	Skew angle for each step θ_{skew_step}	-	-	-	-	5 deg.	3.5 deg.	2.5 deg.	2 deg.	4 deg.	8 deg.
No-load	Cogging torque	0.468 Nm	0.012 Nm	0.081 Nm	0.023 Nm	0.185 Nm	0.124 Nm	0.064 Nm	0.017 Nm	0.166 Nm	0.166 Nm
	Magnetic flux generated by PM	80.9 mWb	80.0 mWb	80.8 mWb	80.0 mWb	80.2 mWb	80.0 mWb	80.1 mWb	80.0 mWb	0.079 mWb	0.079 mWb
	THD of voltage	9.52%	4.07%	4.49%	4.12%	4.82%	4.11%	4.19%	4.17%	4.19%	4.19%
	Iron loss	55.0 W	54.8 W	54.7 W	55.7 W	55.8 W	56.6 W	55.7 W	56.2 W	56.7 W	56.7 W
On-load, 7200 rpm, 10 Arms, $\beta = 0$ deg.	Average torque	4.18 Nm	4.15 Nm	4.17 Nm	4.14 Nm	4.15 Nm	4.14 Nm	4.14 Nm	4.14 Nm	4.12 Nm	4.09 Nm
	Torque ripple	21.0%	11.0%	12.0%	11.4%	16.4%	13.3%	12.5%	11.7%	12.4%	11.7%
	THD of voltage	9.07%	3.88%	4.29%	3.93%	4.59%	3.92%	4.00%	3.98%	3.97%	6.03%
	Iron loss	60.0 W	57.8 W	56.7 W	58.4 W	58.3 W	58.2 W	58.1 W	58.2 W	58.4 W	58.0 W
	L_d, L_q	1.30 mH	1.28 mH	1.27 mH	1.28 mH	1.28 mH	1.28 mH	1.28 mH	1.28 mH	1.28 mH	1.28 mH
	Axial force	0.00 N	-0.89 N	-7.17 N	0.00 N	-0.42 N	-0.59 N	-0.63 N	-0.74 N	0.01 N	0.00 N
	Coil resistance	143.1 m Ω	143.1 m Ω	145.3 m Ω	143.1 m Ω	143.1 m Ω	143.1 m Ω	143.1 m Ω	143.1 m Ω	143.1 m Ω	143.1 m Ω

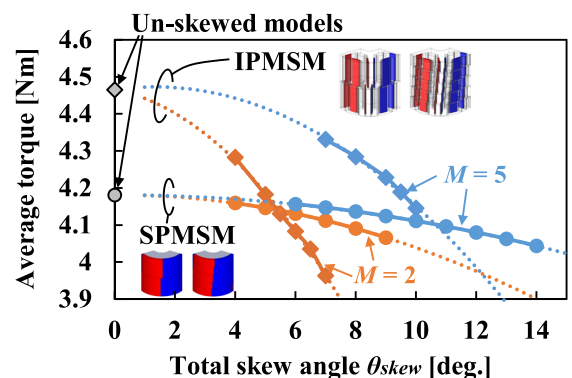
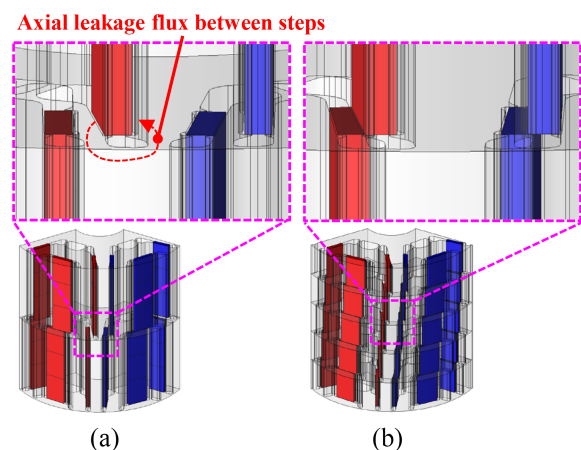
that minimizes the cogging torque is selected. However, all models are able to reduce the THD to less than half compared to the unskewed model.

The linear continuous skew (#1) model also has the smallest torque ripple under on-load condition. However, it does not have as much of a reduction effect as the cogging torque. This is because the skew angle θ_{skew} at which the cogging torque and torque ripple are at their minimums is different, as shown in Fig. 20. There is no significant difference in iron loss and the d -axis and q -axis inductances L_d and L_q due to the skew structure. The linear continuous skew (#2) model for the stator is relatively effective in reducing cogging torque but the axial force F_z is the largest. However, it is effective in cases where it is difficult to provide a continuous skew in the rotor, such as in IPMSM.

E. DIFFERENCE BETWEEN SPMSM AND IPMSM

Fig. 25 compares the changes in average torque of the SPMSM and IPMSM with respect to the skew angle θ_{skew} in the linear step skew (#5). For each model, the models with $M = 2$ and $M = 5$ are plotted. The IPMSM has a larger decrease in average torque when the skew angle θ_{skew} increases. In addition, the effect of the number of steps M is significantly larger for the IPMSM. For $M = 2$, the torque of the IPMSM is 6.8% higher in the unskewed models, but when $\theta_{skew} = 5^\circ$, the difference between both models almost disappears.

Fig. 26 shows the details of the IPMSM model for $M = 2$ and $M = 5$. For $M = 2$, $\theta_{skew_step} = 5^\circ (= \theta_{skew})$, the end of the magnet faces the LSS, as shown in Fig. 26(a). As a result, the axial leakage flux occurs between the steps. On the other hand, when $M = 5$, θ_{skew} is 8° but θ_{skew_step} is 2° , and therefore, the axial leakage magnetic flux between steps can


FIGURE 25. Comparison of average torque between SPMSM and IPMSM with respect to total skew angle in the linear step skew (#5).

FIGURE 26. Difference in axial leakage flux due to skew angle in IPMSM. (a) $M = 2$ and $\theta_{skew} = 5^\circ$. (b) $M = 5$ and $\theta_{skew} = 8^\circ$.

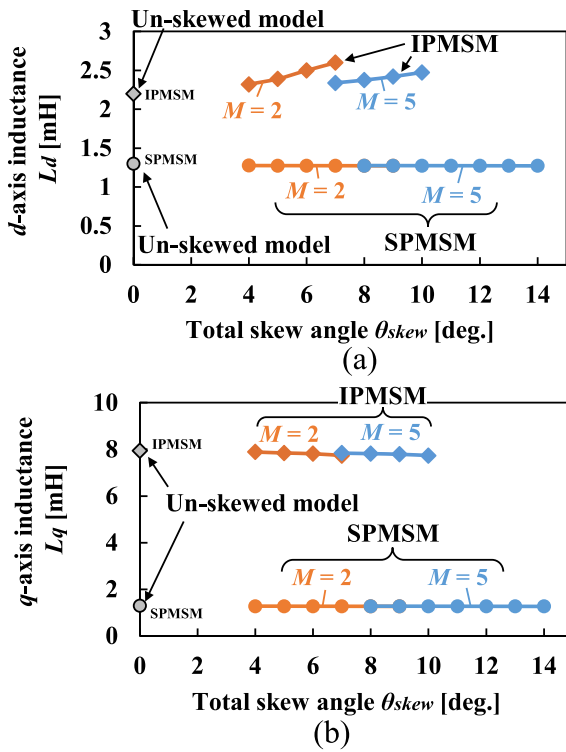


FIGURE 27. dq -axis inductances versus skew angle in SPMSM and IPMSM with $M = 2$ and 5. (a) d -axis inductance L_d . (b) q -axis inductance L_q .

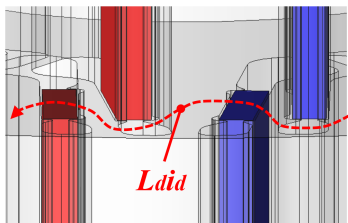


FIGURE 28. Cause of increase in the d -axis inductance when employing skew in IPMSM.

be suppressed. However, the axial leakage magnetic flux of the magnet is still larger than that of the SPMSM. Hence, the decrease in the magnet torque due to skew is greater.

Fig. 27 shows the change in dq -axis inductances L_d and L_q for the SPMSM and IPMSM with respect to the skew angle θ_{skew} . For the SPMSM, L_d and L_q are equal and remain constant even when the skew angle θ_{skew} changes. In contrast, for the IPMSM, L_d rises markedly when the skew angle θ_{skew} increases. As a result, when the skew angle θ_{skew} increases, the salient pole ratio decreases and the reluctance torque decreases. From the above, when the IPMSM employs the skew, both the magnet torque and the reluctance torque decrease, and the average torque is more affected than with the SPMSM. Fig. 28 shows an enlarged view between steps of the IPMSM with $M = 2$ and $\theta_{skew} = 5$. PMs normally have a large magnetic resistance, but as shown by the arrows in Fig. 28, the magnetic flux generated by the armature current

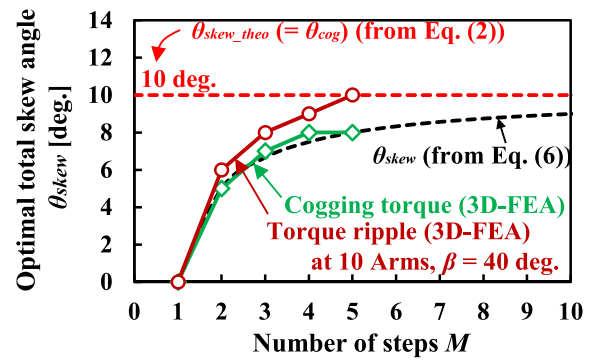


FIGURE 29. Comparison between theoretical skew angle θ_{skew_theo} calculated by equations and optimal skew angle θ_{skew} obtained by 3D-FEA for each number of steps M in IPMSM.

passes between the steps. Consequently, when the skew is used, L_d likely to become larger.

Fig. 29 compares the theoretical skew angle θ_{skew_theo} and the skew angle θ_{skew} for each number of steps M obtained by (2) and (6) with the skew angle at which the cogging torque and torque ripple of the IPMSM are minimum by 3D-FEA. As with the SPMSM, the skew angle for the cogging torque matches the theoretical value well but an error occurs for the torque ripple. In the case of the IPMSM, this is also due to the difference in the magnitude of each frequency component of the cogging torque and the torque ripple.

V. RECENT ADVANCES IN SKEWING TECHNOLOGY AND PROPERTIES IN EACH CATEGORY

Various skew structures have been developed in recent decades, and this section introduces their characteristics and state-of-the-art technologies in each category.

A. CONTINUOUS SKEW (CATEGORIES: #1 TO #4 IN FIG. 3)

In general, the continuous skew is more effective in reducing the cogging torque than the step skew. Zoń et al. [62] compared the cogging torque of PMSMs with a step skew, a continuous skew, and PMs with modified shapes, and the continuous skew showed the highest reduction effect. Continuous skews have the advantage that all frequency components of the cogging torque can be reduced because the angle is changed seamlessly, although this type of skew is difficult to manufacture due to its structure. The IPMSM structure (#1) that uses a continuous skew in the rotor is particularly difficult to manufacture and has few applications [see Fig. 5(b)]. Therefore, category #1 models are often used in SPMSMs and can be realized by skew magnetization using a dedicated magnetizer [63]. Furthermore, because providing a skew causes an imbalance in the magnetic flux in the axial direction, Kang et al. [64] analyzed and measured the electromagnetic force of a skewed SPMSM (see Fig. 30). Skewed structures using additive manufacturing (AM) are also being considered in IPMSMs to improve manufacturability. Urbanek et al. [65] manufactured a continuous skew IPMSM using AM (see

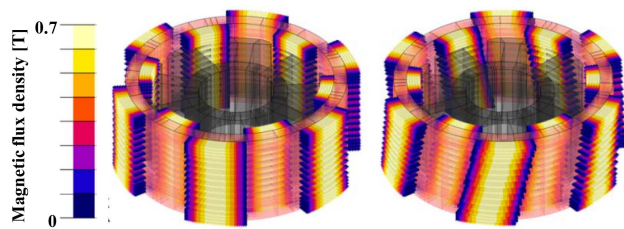


FIGURE 30. Magnetized pattern of rectangular PM (left) and skewed PM (right) [64].

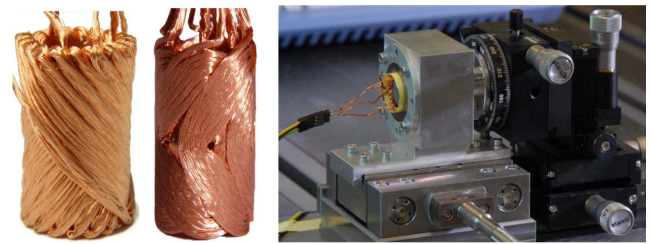


FIGURE 32. Photographs of continuously skewed winding (left) and herringbone winding (right) for slot-less PMSM [69].



FIGURE 31. Sectional view of CAD model (left) and photograph of functional model after production (right) [65].

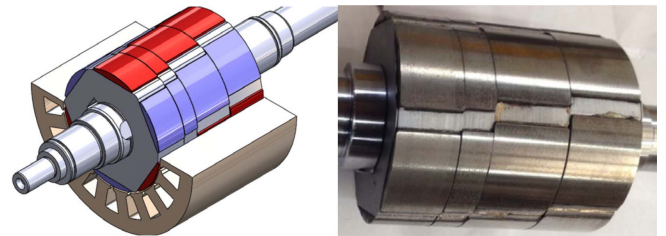


FIGURE 33. Variable step length and variable skew angle model (left) and photograph of the prototype of a skewed rotor [70].

Fig. 31) and demonstrated experimentally that torque ripple was reduced compared with a step skew structure.

In contrast, PMSMs using a continuous skew in the stator are widely used because the stators do not contain PMs, and thus can be manufactured relatively easily, even if a continuous skew is used. Losses of a PMSM with a continuous skew have been analyzed in detail using 3D-FEA. Ohguchi et al. [66] showed that a stator continuous skew model can reduce the stator loss better than a rotor step skew. Furthermore, Koo et al. [67] found that compared with a PMSM without a skew, a continuous stator skew can reduce the eddy current density of the rotor PM and PM loss. Han et al. [68] revealed that vibration can be reduced by a continuous stator skew.

Continuous skews include the herringbone skew in which the direction of displacement changes midway through in the axial direction (#3, #4). The herringbone skew structure has the advantage of suppressing the electromagnetic force in the axial direction because it can be symmetrical in the axial direction [17], [38]. Examples of using a herringbone skew for the IPMSM rotor have been reported but it is generally difficult to manufacture [16]. In addition, Looser et al. [69] reported a PMSM with a structure in which the stator has a herringbone skew (#4) but a slotless stator was used to make the winding easier to configure (see Fig. 32).

B. STEP SKEW (CATEGORIES: #5 TO #13 IN FIG. 3)

The step skew is easy to manufacture and is often used as the rotor skew for both SPMSMs and IPMSMs [see Fig. 5(a) and (b)]. As shown in Section III, the skew angle and axial length of each step are generally constant. However, the cogging torque reduction effect can be enhanced further by varying the axial length of each step (see Fig. 33) [70]. Moreover, when there is a step skew in IPMSMs, leakage magnetic flux between steps is likely to become a problem [71]. Core skew

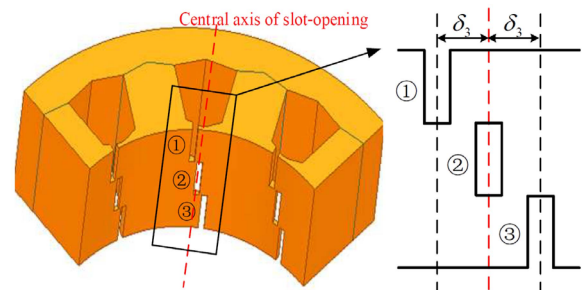


FIGURE 34. Stator model with stepped slot-opening shift (three steps) [72].

structures (#6, #9, and #12) that achieve skew through the shape of the rotor core without changing the position of the PMs are being studied [21]. Stators with a core skew have also been investigated (see Fig. 34). The slot area is the same in the axial direction in this structure, improving the manufacturability of windings compared with the entire skew on the stator core [72]. δ_n is the theoretical shift angle of the tooth-tips. However, depending on the theoretical shift angle δ_n , it may not be possible to insert the winding from the inner circumference of the stator [24].

Similarly, a herringbone step skew can reduce the electromagnetic force in the axial direction [23], [73]. Zhou et al. [73] reported that the herringbone structure shown in Fig. 35 suppresses axial electromagnetic force, reduces the torque ripple, and suppresses the THD of back EMF. Zigzag step skews (#11 to #13), in which steps are stacked alternately, are also effective in suppressing axial electromagnetic forces [74], [75]. Due to the leakage magnetic flux between steps, the average torque tends to be smaller than that for herringbone



FIGURE 35. Rotors with step herringbone skew (left) and without skew (right) [73].

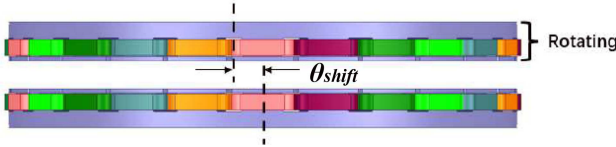


FIGURE 36. Shifted stators of an axial flux machine [29].

skews [74]. However, using a zigzag skew in the stator PM of a DC motor can suppress torque reduction more than a typical skew [26].

C. OTHER SKEWS (CATEGORIES: #14 TO #18 IN FIG. 3)

In PMSMs that have multiple stators or rotors, the multigap skew structure produces a skew effect by shifting the positional relationship (#14 [28] and #15 [29]). Fig. 36 shows an axial flux machine with a double stator structure, in which the angle θ_{shift} of the stator is shifted in the rotation direction [29]. In a multigap skew structure, the optimal skew angle can be calculated by setting $M = 2$ in (6). In [28], the theoretical skew angle of the multigap skew is expressed by the following equation:

$$\theta_{\text{shift}} = \frac{1}{2} \theta_{\text{slot}} \quad (12)$$

where θ_{slot} is the angle of the slot pitch. In addition, a slight skew effect can be obtained even with a normal structure because the angle of the rotor poles and each stator slot is different in the axial flux machine. There have also been reports of axial flux machines with the skew technique but most of them are related to the shape of the rotor magnet [76], [77]. In addition, axial flux machines often use soft magnetic composite for the stator core, which is different from the material used in radial flux machines [78].

The asymmetric skew structure achieves a skew effect by changing the structure of each magnetic pole (#16 [79]). Fig. 37(a) shows the asymmetric structure method proposed by Peng et al. [79], which achieves lower torque ripple than the step skew. The proposed motor combines the asymmetric structure and a segment rotor. Here, α_a and α_b are wider and narrower pole widths in asymmetric pole rotor, respectively. In addition, α_c is the width between magnetic poles. They also conducted actual measurements of vibrations and found that noise frequencies could be removed from the human audible range. Fig. 37(b) shows comparison of torque waveform between a rotor step skew and the proposed models. The

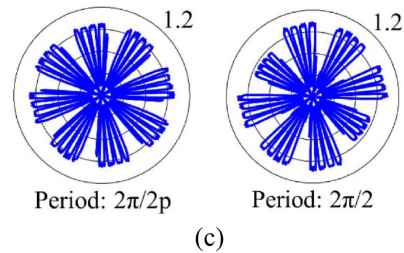
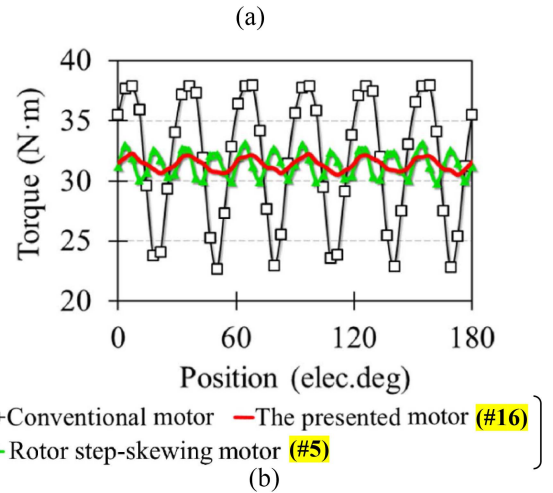
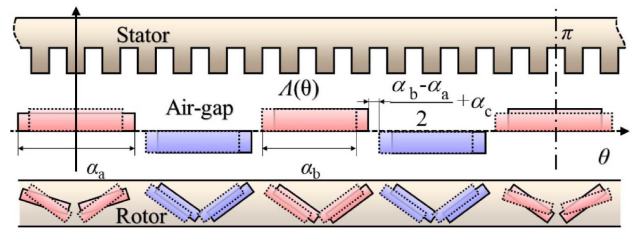


FIGURE 37. Asymmetric skew structure of PMSM [79]. (a) Rotor scheme and superimposed magnetomotive force. (b) Comparison of torque waveforms. (c) Magnitude of magnetic flux density B_r^2 of the rotor step skew model (left) and the proposed model (right).

proposed model achieves lower torque ripple than that of the conventional rotor step skew model. However, the asymmetric skew structure induces the low-order harmonics in the air gap magnetic flux density, as shown in Fig. 37(c).

Skews using magnets with special shapes (#17) have been proposed. Singh et al. [32] manufactured a sinusoidal-petal-shaped PM using AM (see Fig. 38), and experimental results showed that the cogging torque could be reduced compared with the linear continuous skew. Hong et al. [39] showed that making the break in the step skew a continuous skew (see Fig. 39) made the change in magnetic flux gentler and reduced the THD of the back EMF and radial force compared with the step skew. In addition, Ren et al. [80] proposed a structure (#18) in which there is a skewed notch at the tip of the stator core. The cogging torque was reduced more by alternating the direction of the notch skew (see Fig. 40), as in the herringbone skew, than by keeping the direction constant.

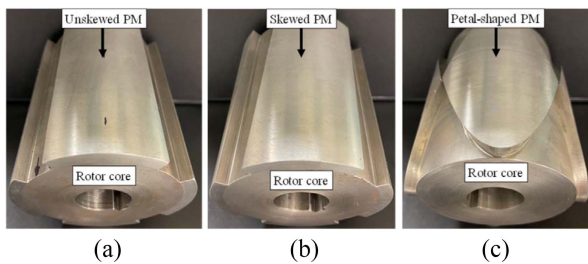


FIGURE 38. Photographs of the prototype of rotor with cold-spray NdFeB PM fabricated by AM. (a) Without skew. (b) Conventional linear skew. (c) Proposed sinusoidal-petal-shaped PM [32].

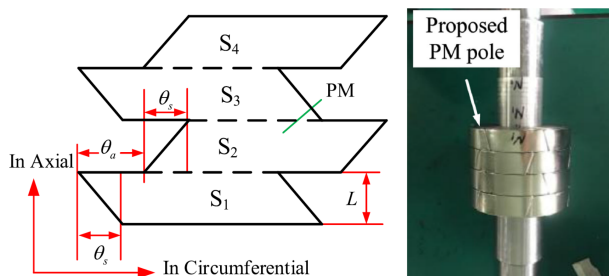


FIGURE 39. Concept of piecewise staggered poles with continuous skew (left) and photograph of prototype (right) [39].

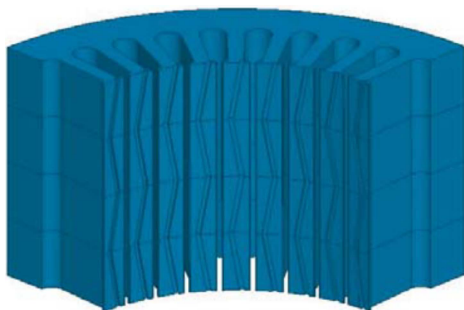


FIGURE 40. Stator using teeth notching with a skew in alternating directions [80].

Other structures that have been reported to reduce the torque ripple include conical motors [81]. However, even if the rotor and stator are made conical structure, the phase of the torque waveform does not change much, and hence, the effect of reducing the cogging torque and torque ripple tends to be smaller than with the skew technique. In addition, the conical structure has the issue of poor manufacturability because the surface needs to be continuously changed. However, conical motors are suitable when it is necessary to balance the external force in the axial direction [82].

D. ANALYSIS METHOD AND ACCURACY

PMSMs containing a skew have a different structure in the axial direction; thus, it is desirable to analyze the structure using 3D-FEA. However, 3D-FEA is time consuming, so many research groups are considering methods to predict

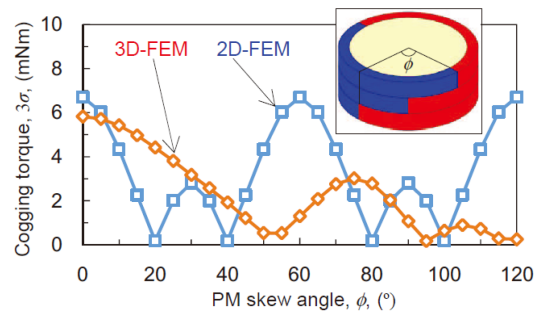


FIGURE 41. Comparison of optimal skew angle for 2-D and 3D-FEA [86].

skew characteristics using 2D-FEA or mathematical models. Mohr et al. [13] proposed a method using a multislice technique with 2D-FEA to shorten the analysis time. In addition, Lazari et al. [83] proposed a method that includes the dq -axis cross-coupling and the magnetic saturation in 2D-FEA that considers the skew. This method not only shortens analysis time but also enables accurate prediction of skew characteristics under heavy loads where magnetic saturation occurs. A mathematical model has been developed to predict skew characteristics faster than 2D-FEA and the results closely matched the 2D-FEA results [55], [84].

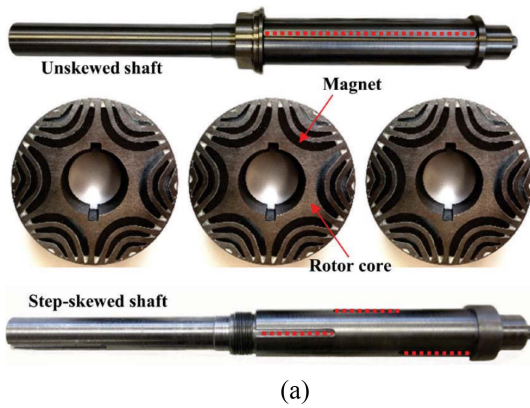
Predicted characteristics of PMSMs with a skew are likely to have large errors between 2D-FEA and 3D-FEA. Errors tend to increase for step skews, and the main cause of this is leakage magnetic flux between steps [85]. Consequently, Asama et al. [86] described that the optimal skew angles for 2D-FEA and 3D-FEA are significantly different (see Fig. 41). Therefore, it is difficult to evaluate the characteristics using 2D-FEA in structures that have large leakage flux in the axial direction.

In Fig. 41, for $N_p = 2$, $N_s = 12$, and $M = 3$, when the optimal skew angle is calculated using (6), $\theta_{\text{skew}} = 20^\circ$, which matches the optimal skew angle calculated by 2D-FEA. However, in practice, the optimum skew angle changes from the theoretical value due to the axial leakage flux and the end effect. Another example in which the skew angle at which the cogging torque reaches its minimum different in 3D-FEA from the theoretical value has also been reported [72].

In contrast, for IPMSMs, because there is a core in the rotor, leakage flux in a step skew tends to increase depending on the structure, and Fig. 42 compares the 2D-FEA, 3D-FEA, and experimental results in an IPMSM with a step skew [87]. The 3D-FEA and experimentally measured voltages agreed well [see Fig. 42(b)]. However, there are large errors between the 2D-FEA and experimental results, especially in the fundamental wave. Therefore, it is possible to predict the skew characteristics roughly using 2D-FEA but there are errors in the optimal skew angle and skew characteristics due to the axial leakage flux and end effects.

E. PATENTS RELATED TO PMSM USING SKEW

As shown in Fig. 2, various patents related to the skew have been published to date. Academic papers often investigate



(a)

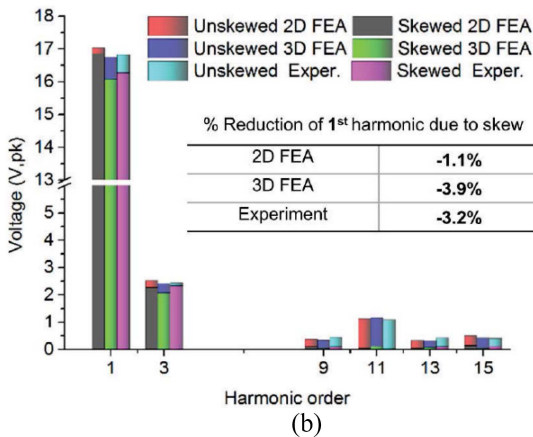


FIGURE 42. Comparison of FEA-predicted results and experimental results [87]. (a) Prototype rotor stacks with three-step-skewed and unskewed shafts. (b) Back EMF harmonics.

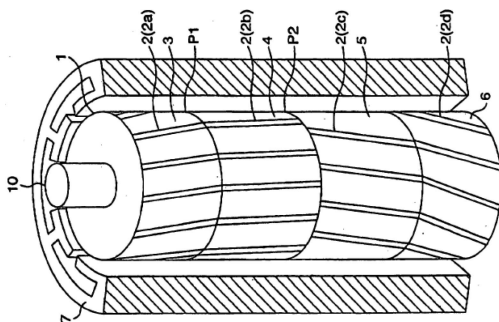


FIGURE 43. Structure that combines the continuous skew and the step skew [88].

topologies using the skew, but patents published by motor manufacturers are characterized by a large amount of content related to manufacturing, especially in the case of stators.

Fig. 43 shows a structure that combines the continuous skew and the step skew. This structure is basically a step skew of $M = 4$, but the continuous skew is adopted within each step, and the skew angle θ_{skew} and direction are different for each step. As a result, it is possible to reduce the torque ripple

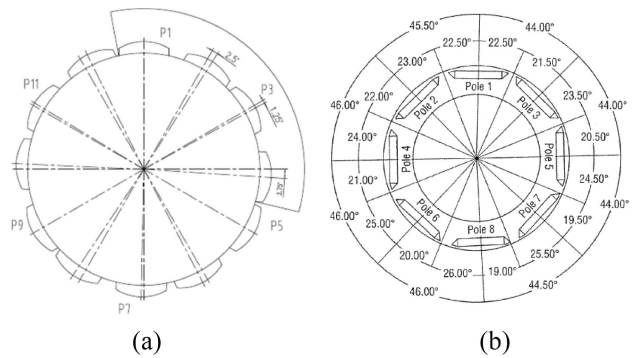


FIGURE 44. Asymmetric skew structures. (a) SPMSM [89]. (b) IPMSM [90].

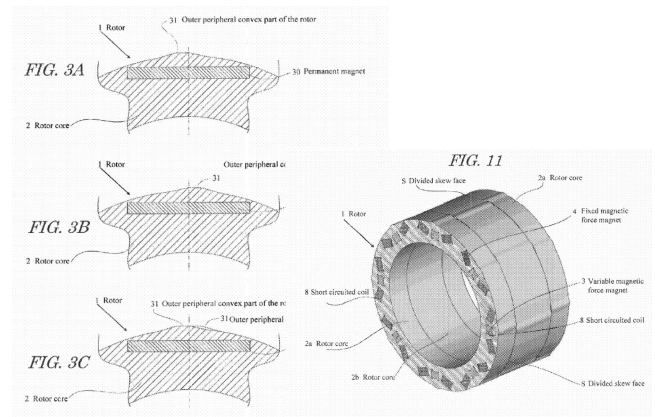


FIGURE 45. Novel rotor core skew structure for IPMSM [91].

under on-load condition to almost zero with a small number of steps M [88].

Fig. 44 shows patents for asymmetric skew in SPMSM and IPMSM, respectively. In the case of the SPMSM in Fig. 44(a), the installation angle of each PM is changed [89]. It can be manufactured in the same way as typical SPMSMs, and achieves a high cogging torque reduction effect and noise reduction. In the case of the IPMSM in Fig. 44(b), the torque ripple can be reduced while maintaining the average torque by changing a pole arc angle [90]. In addition, it has excellent manufacturability because it can be manufactured in the same way as typical IPMSMs. However, the disadvantage is that the shape of the PM differs depending on the magnetic pole.

In Fig. 45, the rotor is divided in the axial direction and a protrusion is provided on the rotor surface. The position of the protrusion can be changed in each step to obtain a skew effect. In addition, PMs can be configured by a single tabular member that penetrates axially divided steps due to this structure [91].

As discussed in the 3D-FEA results in Section IV, the step skew reduces the effective magnetic flux ψ_{pm} due to the axial leakage flux between each step. Furthermore, in IPMSM, the reluctance torque also decreases due to the increase in d -axis inductance. To prevent this deterioration, it has been proposed to provide an air gap between each step in various step skew

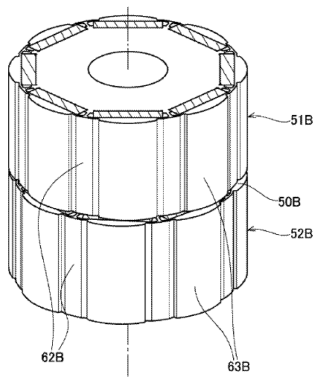


FIGURE 46. Step skew structure employing air gap between steps [92].

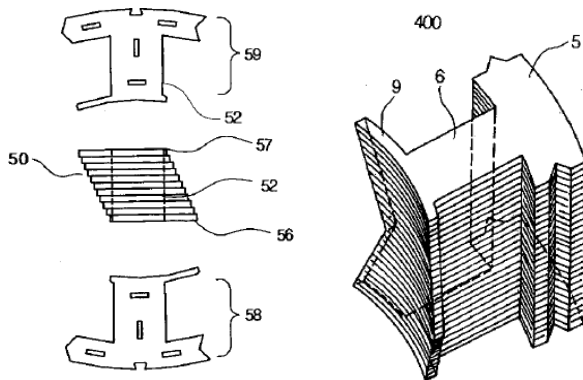


FIGURE 47. Example of stator continuous skew structure to only tooth-tips while maintaining manufacturability [95].

structures [92], [93], [94], [95]. Fig. 46 is an example of an IPMSM, where the reduction in average torque can be suppressed by providing an air gap between the steps [92]. In addition, the insertion of nonmagnetic material between the steps has also been considered. It has been reported that the resistance to demagnetization of PMs can be improved by increasing the distance between steps in IPMSM [93].

Fig. 47 shows a structure with the continuous herringbone skew (#4) on the stator [96]. This patent reports a new punching method using a punching die for a split stator core to achieve the skew. By making only the tooth-tip of the stator core a different shape in the axial direction, the skew effect can be obtained while maintaining an unskewed winding area. As a result, it is possible to wind coils in an aligned manner while employing the skew on the stator [96].

Fig. 48 shows a patent on the manufacture of continuous stator skew cores. According to this patent, each skew core can be integrally molded with thermosetting resin and easily assembled by the insert molding method. As a result, even if a skew core is employed, the coil winding process is easy by adopting a split core structure [97].

Fig. 49 shows a patent on a manufacturing method for a structure that combines magnetic wedges and the skew to reduce torque ripple. Open slots are more suitable for installing

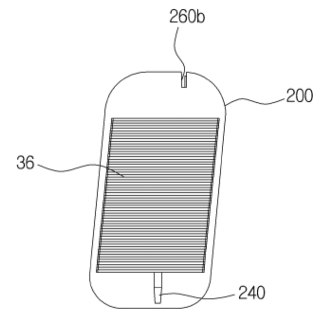


FIGURE 48. Stator skew core integrally molded with thermosetting resin [97].

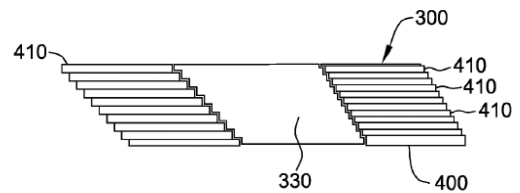


FIGURE 49. Skewed stator core with magnetic wedges between teeth. [98].

windings, but the torque ripple becomes large. In such a case, torque ripple is reduced by combining magnetic wedges with the skew while maintaining manufacturability [98].


VI. DISCUSSION

This section compares and discusses each skew category based on the 3D-FEA results in Section IV and information from many references and patents. Tables 4 and 5 provide a comprehensive comparison of each skew category for SPMSM and IPMSM, respectively. The main difference between SPMSM and IPMSM is that in categories #1 and #3, SPMSM can be realized by using a corresponding magnetizer, but it is difficult to adopt in IPMSM because PMs are inserted into the core.

In addition, when a continuous skew is employed in the stator as in #2 in both cases, although the torque ripple reduction effect is high, it is difficult to automate the winding operation because of a twisted core. As a result, the cost increases, making alignment winding difficult. Therefore, the space factor also decreases, and there is a high possibility that the copper loss will increase. In addition, this skew structure has a large axial force F_z acting on the rotor, so the burden on the bearing is also large.


In both SPMSM and IPMSM, segment-type step skews (#5, #8, #11) are widely used because they are more feasible, although they are more expensive than typical motors. Herringbone skews (#8) and zigzag skews (#11) are used to suppress the axial force F_z . However, linear skews (#5) are more effective at reducing cogging torque. However, the step skew may require additional dies to change the position of the key grooves, which increase manufacturing costs [99]. In addition, the continuous skew requires mechanisms to control

TABLE 4 Comparison of Each Skew Category in SPMSM

Skew type for SPMSM 			Category No.	Cost	Manufacturability	Applicability	Torque ripple	Average torque	Axial leakage flux	Axial force	Noise and vibration	Loss	Rotor stress	
Continuous skew	Linear	Rotor	#1	○	○	⊙	⊙	⊙	⊙	△	△	○	⊙	
		Stator	#2	△	△	○	⊙	⊙	⊙	×	△	△	⊙	
	Herring bone	Rotor	#3	○	△	○	⊙	⊙	⊙	⊙	○	○	⊙	
		Stator	#4	×	×	△	⊙	⊙	⊙	⊙	○	△	⊙	
Step skew	Linear	Segment	#5	○	○	⊙	○	⊙	⊙	□	□	○	⊙	
		Core skew	#6	⊙	⊙	⊙	⊙	⊙	⊙	⊙	□	□	○	
		Stator	#7	×	×	×	○	⊙	○	△	□	△	⊙	
		Stator	#8	○	○	⊙	○	○	○	⊙	○	○	○	⊙
	Herring bone	Segment	#9	⊙	⊙	⊙	○	⊙	○	⊙	○	○	○	⊙
		Core skew	#10	×	×	×	○	□	△	○	○	○	△	⊙
		Stator	#11	○	○	⊙	○	○	○	○	○	○	○	⊙
		Stator	#12	×	×	×	○	□	△	○	○	○	△	⊙
Zigzag	Segment	#13	○	○	⊙	○	○	○	○	○	○	○	⊙	
	Core skew	#14	×	×	×	○	□	△	○	○	○	△	⊙	
	Stator	#15	○	○	⊙	△	○	⊙	⊙	⊙	△	△	○	
	Stator	#16	□	○	⊙	△	○	⊙	⊙	⊙	△	△	⊙	
Other skews	Multi-gap	Rotor	#17	⊙	⊙	⊙	△	○	⊙	⊙	△	△	○	
		Stator	#18	□	○	⊙	△	○	⊙	⊙	△	△	⊙	
	Asymmetric		#19	⊙	⊙	⊙	○	⊙	⊙	⊙	×	×	□	
	Novel PM		#20	△	△	⊙	○	□	⊙	⊙	□	□	○	
Notch skew		#21	△	△	⊙	○	□	⊙	⊙	△	△	⊙		

(⊙ : Very good ○ : Good □ : Average △ : Below average × : Poor)

TABLE 5 Comparison of Each Skew Category in IPMSM

Skew type for IPMSM 			Category No.	Cost	Manufacturability	Applicability	Torque ripple	Average torque	Axial leakage flux	Axial force	Noise and vibration	Loss	Rotor stress	
Continuous skew	Linear	Rotor	#1	×	×	×	⊙	⊙	⊙	△	△	○	×	
		Stator	#2	△	△	○	⊙	⊙	⊙	×	△	△	⊙	
	Herring bone	Rotor	#3	×	×	×	⊙	⊙	⊙	⊙	○	○	×	
		Stator	#4	×	×	△	⊙	⊙	⊙	⊙	○	△	⊙	
Step skew	Linear	Segment	#5	⊙	⊙	⊙	○	○	○	□	□	○	⊙	
		Core skew	#6	△	⊙	△	□	⊙	⊙	⊙	□	□	○	
		Stator	#7	×	×	×	○	⊙	○	△	□	△	⊙	
		Stator	#8	⊙	⊙	⊙	○	□	○	⊙	○	○	○	⊙
	Herring bone	Segment	#9	△	⊙	△	□	○	⊙	⊙	○	○	○	⊙
		Core skew	#10	×	×	×	○	□	△	○	○	○	△	⊙
		Stator	#11	⊙	⊙	⊙	○	□	○	○	○	○	○	⊙
		Stator	#12	△	⊙	△	□	○	⊙	⊙	○	○	○	⊙
Zigzag	Segment	#13	×	×	×	○	□	△	○	○	○	△	⊙	
	Core skew	#14	△	△	⊙	△	○	⊙	⊙	⊙	△	△	□	
	Stator	#15	□	○	⊙	△	○	⊙	⊙	⊙	△	△	⊙	
	Stator	#16	⊙	⊙	⊙	○	⊙	⊙	⊙	⊙	×	×	△	
Other skews	Multi-gap	Rotor	#17	△	△	⊙	△	○	⊙	⊙	△	△	⊙	
		Stator	#18	□	○	⊙	△	○	⊙	⊙	△	△	⊙	
	Asymmetric		#19	⊙	⊙	⊙	○	⊙	⊙	⊙	×	×	△	
	Novel PM		#20	△	△	⊙	○	□	⊙	⊙	□	□	○	
Notch skew		#21	△	△	⊙	○	□	⊙	⊙	△	△	⊙		

(⊙ : Very good ○ : Good □ : Average △ : Below average × : Poor)

the positions of the welding or caulking points to fix the LSSs, which also increases manufacturing costs [100], [101].

Among other skews, asymmetric skews are superior in terms of cost and manufacturability because they can be manufactured in the same way as typical motors. However, costs increase when the shape of the PM is changed depending on the magnetic pole. Furthermore, asymmetric skews also

generate low-order harmonics, which raises concerns about iron loss, etc.

Finally, the advantages and disadvantages of each category of skew are summarized in Table 6. Each model has different strengths and weaknesses, respectively. It is necessary to select an appropriate skew structure for each application, taking these properties into account.

TABLE 6 Comparative Analysis of Advantages and Disadvantages in PMSM Using Skewing Technology

Category No.	Advantages	Disadvantages
#1	- Highly effective in reducing torque ripple and cogging torque - Less axial leakage flux	- Difficult to manufacture, especially in IPMSMs - Large axial electromagnetic force due to asymmetry in the axial direction
#2	- Highly effective in reducing torque ripple and cogging torque - Applicable to IPMSMs	- Winding becomes longer, and resistance and copper loss increase - Extremely large axial electromagnetic force due to asymmetry in the axial direction
#3	- Axially symmetric, with small axial electromagnetic force and long bearing life	- Manufacturing of IPMSMs is extremely difficult because magnets cannot be inserted - Difficult to magnetize PMs even for SPMSMs
#4	- Axially symmetric, with small axial electromagnetic force and long bearing life	- Extremely difficult to manufacture from the perspective of winding placement
#5	- Good manufacturability among skew structures - Axial leakage flux is less likely to occur because θ_{skew_step} can be made small even with a small number of steps M	- Large axial electromagnetic force due to asymmetry in the axial direction
#6	- Permanent magnets can be placed uniformly in the axial direction (namely, without skewed PM) - Less axial leakage flux	- Die for laminated steel sheet becomes larger - Large axial electromagnetic force due to asymmetry in the axial direction - Few applicable structures
#7	- No axial leakage flux occurs in the rotor	- Large axial electromagnetic force due to asymmetry in the axial direction - Difficult to install winding, and low coil space factor
#8	- Axial symmetry can suppress electromagnetic force regardless of the number of steps M and can extend bearing life	- When the number of steps M is small, θ_{skew_step} becomes large and the axial leakage flux becomes large
#9	- Axial symmetry can suppress electromagnetic force regardless of the number of steps M and can extend bearing life - Less axial leakage flux	- Die for laminated steel sheet becomes larger - Few applicable structures
#10	- Axial symmetry can suppress electromagnetic force regardless of the number of steps M and can extend bearing life - No axial leakage flux occurs in the rotor	- Die for laminated steel sheet becomes larger - Difficult to install winding, and low coil space factor - Large magnetic flux leakage at tooth-tips
#11	- When the number of steps M is an odd number, the rotor is symmetrical in the axial direction, which suppresses electromagnetic force and extends the bearing life	- When the number of steps M is small, θ_{skew_step} becomes large and the axial leakage flux becomes large
#12	- When the number of steps M is an odd number, the rotor is symmetrical in the axial direction, which suppresses electromagnetic force and extends the bearing life - Less axial leakage flux	- Die for laminated steel sheet becomes larger - Few applicable structures
#13	- When the number of steps M is an odd number, the rotor is symmetrical in the axial direction, which suppresses electromagnetic force and extends the bearing life - No axial leakage flux occurs in the rotor	- Die for laminated steel sheet becomes larger - Difficult to install winding, and low coil space factor - Large magnetic flux leakage at tooth-tips
#14	- Skew can be easily achieved by simply shifting the positions of the two rotors	- Electromagnetic forces of the two rotors cannot be canceled out, resulting in loud noise and vibration - The number of steps M is equal to the number of rotors - Installation in the motor case is difficult
#15	- Easy to install because the stator is on the outside	- Electromagnetic forces of the two stators cannot be canceled out, resulting in loud noise and vibration - The number of steps M is equal to the number of stators
#16	- This structure can be manufactured in the same way as typical IPMSMs and SPMSMs without skew, making it the most manufacturable	- Low-order harmonic magnetic flux is generated, resulting in large iron loss, vibration, and noise
#17	- Extremely high degree of design freedom	- Special techniques such as AM are required
#18	- High degree of design freedom	- Difficult to manufacture - A special die for laminated steel sheet is required

VII. SUMMARY AND CONCLUSION

This article has provided an overview of PMSMs using skewing techniques and recent trends. First, PMSMs using a skew are classified into 18 categories and are described the characteristics of each. This article also statistically discussed the usage rate and purposes of each structure, and then summarized and discussed the results in Figs. 4 and 5. The main purpose of a skew is to reduce the cogging torque and torque ripple but skews have also been used to reduce noise and vibration. Furthermore, some studies concluded that skews are effective in suppressing the shaft voltage and improving startup characteristics.

This article discussed the theoretical skew angle and visualized it using an example of a PMSM with 8 poles and 48 slots. Although the skew angle has been defined in various papers, the definitions differ, so this article summarized the

definition in an easy-to-understand manner. The skew factor was visualized and its relationship with the theoretical formula for the skew angle was explained. In Section IV, 3D-FEA results of various PMSMs employing the skew for quantitative comparison are shown. Furthermore, the difference in the effect of the skew on SPMSM and IPMSM was clarified using 3D-FEA. In Section V, the characteristics of skew structures in each category and the latest trends are introduced. It has been difficult to use a continuous skew in the rotor of IPMSMs but research has been conducted to achieve this using AM. In addition, the number of studies in which skew structures are fabricated by AM is increasing, and it has been reported that PMs with special shapes manufactured using AM had a high skew effect. Finally, in Section VI, this article summarized the advantages and disadvantages of each skew structure based on the results of 3D-FEA and references,

and discussed their characteristics. It is necessary to select the appropriate skew structure according to the application because each structure has different advantages. It is likely that new skewing technologies will continue to be proposed as materials and manufacturing technology develop.

REFERENCES

- [1] A. De Almeida et al., "EuP lot 11 motors, ecodesign assessment of energy using products," ISR-Univ. Coimbra, Brussels, Belgium, EU Rep. 11 Motors, Feb. 2008.
- [2] H. Y. Sun and K. Wang, "Effect of third harmonic flux density on cogging torque in surface-mounted permanent magnet machines," *IEEE Trans. Ind. Elect.*, vol. 66, no. 8, pp. 6150–6158, Aug. 2019.
- [3] D. Wang, C. Peng, J. Li, and C. Wang, "Comparison and experimental verification of different approaches to suppress torque ripple and vibrations of interior permanent magnet synchronous motor for EV," *IEEE Trans. Ind. Elect.*, vol. 70, no. 3, pp. 2209–2220, Mar. 2023.
- [4] S. Wang, J. Hong, Y. Sun, and H. Cao, "Effect comparison of zigzag skew PM pole and straight skew slot for vibration mitigation of PM brush DC motors," *IEEE Trans. Ind. Elect.*, vol. 67, no. 6, pp. 4752–4761, Jun. 2020.
- [5] V. Dmitrievskii, V. Prakht, V. Kazakbaev, and A. Anuchin, "Comparison of interior permanent magnet and synchronous homopolar motors for a mining dump truck traction drive operated in wide constant power speed range," *Mathematics*, vol. 10, no. 9, 2022, Art. no. 1581.
- [6] G. Pellegrino, P. Guglielmi, A. Vagati, and F. Villata, "Core losses and torque ripple in IPM machines: Dedicated modeling and design tradeoff," *IEEE Trans. Ind. Appl.*, vol. 46, no. 6, pp. 2381–2391, Nov./Dec. 2010.
- [7] J.-Y. Choi, Y.-S. Park, and S.-M. Jang, "Experimental verification and electromagnetic analysis for performance of interior PM motor according to slot/pole number combination," *IEEE Trans. Magn.*, vol. 48, no. 2, pp. 987–990, Feb. 2012.
- [8] E. E. Dreesse, "A-C elevator motors of the squirrel-cage type," *Trans. Amer. Inst. Elect. Eng.*, vol. 47, no. 4, pp. 1339–1347, Oct. 1928.
- [9] J. Keränen, P. Ponomarev, J. Pippuri, P. Råback, M. Lyly, and J. Westerglund, "Parallel performance of multi-slice finite-element modeling of skewed electrical machines," *IEEE Trans. Magn.*, vol. 53, no. 6, Jun. 2017, Art. no. 7201204.
- [10] T. M. Jahns, "Torque production in permanent-magnet synchronous motor drives with rectangular current excitation," in *Proc. Annu. Meeting Ind. Appl. Soc.*, Mexico City, Mexico, 1983, pp. 476–487.
- [11] A. K. Pathak et al., "Cerium: An unlikely replacement of dysprosium in high performance Nd-Fe-B permanent magnets," *Adv. Mater.*, vol. 27, no. 16, pp. 2663–2667, 2015.
- [12] D. Li, Y. Xie, F. Liu, W. Cai, and F. Yang, "A novel rotor-step skewing method for vibration mitigation in interior permanent magnet synchronous motor," in *Proc. IEEE Int. Magn. Conf.- Short Papers*, Sendai, Japan, 2023, pp. 1–2.
- [13] M. Mohr, O. Bíró, A. Stermecki, and F. Divoky, "A finite element-based circuit model approach for skewed electrical machines," *IEEE Trans. Magn.*, vol. 50, no. 2, pp. 837–840, Feb. 2014.
- [14] A.-I. Constantin, E. Tudor, D. Marin, C. Dumitru, and M. G. Mihaiescu, "Case studies related to the optimization of a surface mounted permanent magnets synchronous generator applied for a small hydrokinetic turbine," in *Proc. Int. Conf. Expo. Elect. Power Eng.*, Iasi, Romania, 2022, pp. 67–72.
- [15] H. Dhulipati, S. Mukundan, K. L. V. Iyer, and N. C. Kar, "Skewing of stator windings for reduction of spatial harmonics in concentrated wound PMSM," in *Proc. IEEE 30th Can. Conf. Elect. Comput. Eng.*, Windsor, ON, Canada, 2017, pp. 1–4.
- [16] H.-R. Noh, C.-H. Lee, H.-J. Jang, and K.-C. Kim, "A study on the characteristics change according to the type of application of the rotor skew of the interior permanent magnet synchronous motor," in *Proc. 25th Int. Conf. Elect. Mach. Syst.*, Chiang Mai, Thailand, 2022, pp. 1–5.
- [17] G.-J. Park, Y.-J. Kim, and S.-Y. Jung, "Design of IPMSM applying V-shape skew considering axial force distribution and performance characteristics according to the rotating direction," *IEEE Trans. Appl. Supercond.*, vol. 26, no. 4, Jun. 2016, Art. no. 0605205.
- [18] Y. An et al., "Open-circuit air-gap magnetic field calculation of interior permanent magnet synchronous motor with V-shaped segmented skewed poles using hybrid analytical method," *IEEE Trans. Magn.*, vol. 57, no. 12, Dec. 2021, Art. no. 8108309.
- [19] S. Wu, C. Tian, W. Zhao, J. Zhou, and X. Zhang, "Design and analysis of an integrated modular motor drive for more electric aircraft," *IEEE Trans. Transp. Electric.*, vol. 6, no. 4, pp. 1412–1420, Dec. 2020.
- [20] Y. Avsar, A. Fenercioglu, and M. Soyaşlan, "Design optimization of PM synchronous motor: Rail mounted belt drive elevator systems," *IEEE Trans. Ind. Appl.*, vol. 60, no. 1, pp. 301–311, Jan./Feb. 2024.
- [21] D.-W. Nam, K.-B. Lee, H.-J. Pyo, M.-J. Jeong, and W.-H. Kim, "A study on performance improvement by reducing axial force of double-layer spoke-type PMSM with core skew structure," in *Proc. IEEE 20th Biennial Conf. Electromagn. Field Comput.*, Denver, CO, USA, 2022, pp. 1–2.
- [22] D.-W. Nam, D.-H. Kim, I.-J. Yang, S.-W. Song, and W.-H. Kim, "A study on stator shape to reduce cogging torque and torque ripple of double-layer spoke type PMSM," in *Proc. IEEE Energy Convers. Congr. Expo.*, Detroit, MI, USA, 2022, pp. 1–7.
- [23] W. Fei, P. C.-K. Luk, and W. Liang, "Comparison of torque characteristics in permanent magnet synchronous machine with conventional and herringbone rotor step skewing techniques," in *Proc. IEEE Energy Convers. Congr. Expo.*, 2016, pp. 1–8.
- [24] D. Shijo et al., "Manufacturing technology of stator core to reduce torque ripple," *Mitsubishi Denki Giho*, vol. 87, no. 12, pp. 22–25, 2013.
- [25] J. Blum, J. Merwerth, and H.-G. Herzog, "Investigation of the segment order in step-skewed synchronous machines on noise and vibration," in *Proc. 4th Int. Electr. Drives Prod. Conf.*, 2014, pp. 1–6.
- [26] S. Wang, J. Hong, Y. Sun, and H. Cao, "Effect Comparison of zigzag skew PM pole and straight skew slot for vibration mitigation of PM brush DC motors," *IEEE Trans. Ind. Electron.*, vol. 67, no. 6, pp. 4752–4761, Jun. 2020.
- [27] S. Leitner, H. Gruebler, and A. Muetze, "Cogging torque minimization and performance of the sub-fractional HP BLDC claw-pole motor," *IEEE Trans. Ind. Appl.*, vol. 55, no. 5, pp. 4653–4664, Sep./Oct. 2019.
- [28] Y. B. Kim, H. T. Jang, H. S. Choi, C. S. Koh, and P. S. Shin, "A back EMF optimization of double layered large-scale BLDC motor by using hybrid optimization method," *IEEE Trans. Magn.*, vol. 47, no. 5, pp. 998–1001, May 2011.
- [29] Q. Wang, Y. Xu, F. Yu, and M. Sun, "Analysis and reduction of cogging torque in double-stator axial-flux permanent-magnet disk synchronous generator with soft magnetic composite core," in *Proc. 26th Int. Conf. Elect. Mach. Syst.*, 2023, pp. 1011–1015.
- [30] C. Peng, D. Wang, Z. Feng, and B. Wang, "A new segmented rotor to mitigate torque ripple and electromagnetic vibration of interior permanent magnet machine," *IEEE Trans. Ind. Electron.*, vol. 69, no. 2, pp. 1367–1377, Feb. 2022.
- [31] Y. Xiao et al., "A novel asymmetric interior permanent magnet machine for electric vehicles," *IEEE Trans. Energy Convers.*, vol. 36, no. 3, pp. 2404–2415, Sep. 2021.
- [32] S. Singh et al., "Cold-spray additive manufacturing of a petal-shaped surface permanent magnet traction motor," *IEEE Trans. Transp. Electric.*, vol. 9, no. 3, pp. 3636–3648, Sep. 2023.
- [33] D. Wang, X. Wang, and S.-Y. Jung, "Reduction on cogging torque in flux-switching permanent magnet machine by teeth notching schemes," *IEEE Trans. Magn.*, vol. 48, no. 11, pp. 4228–4231, Nov. 2012.
- [34] W. Ren, Q. Xu, Q. Li, and L. Chen, "Reducing cogging torque and suppressing torque ripple in PMSynRM for EV/HEV applications," in *Proc. IEEE Conf. Expo Transp. Electric. Asia-Pacific*, Beijing, China, 2014, pp. 1–6.
- [35] N. Saed, S. Asgari, and A. Muetze, "On the effect of claw geometry on the vibration of single-phase claw-pole BLDC machines," in *Proc. 11th Int. Conf. Power Electron. ECCE Asia*, Jeju Island, South Korea, 2023, pp. 142–147.
- [36] J. Liang, Y. Li, C. Mak, B. Bilgin, D. Al-Ani, and A. Emadi, "A comprehensive analysis of the acoustic noise in an interior permanent magnet traction motor," in *Proc. IEEE Energy Convers. Congr. Expo.*, Baltimore, MD, USA, 2019, pp. 3845–3851.
- [37] C.-H. Song, I.-S. Song, H.-S. Shin, C.-H. Lee, and K.-C. Kim, "A design of IPMSM for high-power electric vehicles with wide-field-weakening control region," *IEEE Trans. Magn.*, vol. 58, no. 2, Feb. 2022, Art. no. 8700305.

- [38] K. Kurihara, H. Yoshino, and K. Shimauchi, "Surface permanent magnet motors with complicated permanent magnet shapes formed by binder-less net shaping process," in *Proc. 21st Int. Conf. Elect. Mach. Syst.*, Jeju, South Korea, 2018, pp. 510–513.
- [39] J. Hong, S. Wang, Y. Sun, X. Sun, and H. Cao, "Piecewise stagger poles with continuous skew edge for vibration reduction in surface-mounted PM synchronous machines," *IEEE Trans. Ind. Electron.*, vol. 68, no. 9, pp. 8498–8506, Sep. 2021.
- [40] B.-T. Kim, D.-K. Kim, B.-I. Kwon, and T. A. Lipo, "Optimal skew angle for improving of start-up performance of a single-phase line-start permanent magnet motor," in *Proc. IEEE Ind. Appl. Soc. Annu. Meeting*, 2008, pp. 1–6.
- [41] X. Gu, X. Wang, L. Sun, B. Peng, L. Xiong, and X. Zhang, "The approach for suppressing intrinsic shaft voltage by segmented skewed poles in permanent magnet synchronous motors," in *Proc. IEEE 6th Int. Elect. Energy Conf.*, Hefei, China, 2023, pp. 1581–1585.
- [42] M. Davoli, C. Bianchini, A. Torreggiani, and F. Immovali, "A design method to reduce pulsating torque in PM assisted synchronous reluctance machines with asymmetry of rotor barriers," in *Proc. 42nd Annu. Conf. IEEE Ind. Electron. Soc.*, Florence, Italy, 2016, pp. 1566–1571.
- [43] 2017. [Online]. Available: <https://mqitechnology.com/wp-content/uploads/2017/09/bonded-neo-magnetization-guide.pdf>
- [44] [Online]. Available: <https://www.magnet-sdm.com/skewed-magnetized-magnet/>
- [45] K.-C. Kim, "A novel method for minimization of cogging torque and torque ripple for interior permanent magnet synchronous motor," *IEEE Trans. Magn.*, vol. 50, no. 2, pp. 793–796, Feb. 2014.
- [46] C. He and T. Wu, "Design and analysis of a V-type fractional-slots IPMSM with distributed winding for electric vehicles," in *Proc. XXII Int. Conf. Elect. Mach.*, Lausanne, Switzerland, 2016, pp. 1459–1465.
- [47] R. Tsunata, K. Izumiya, M. Takemoto, J. Imai, T. Saito, and T. Ueno, "Designing and prototyping an axial-flux machine using ferrite PM and round wire for traction applications: Comparison with a radial-flux machine using Nd-Fe-B PM and rectangular wire," *IEEE Trans. Ind. Appl.*, vol. 60, no. 3, pp. 3934–3949, May/June 2024.
- [48] J. Yun and S. B. Lee, "Influence of aluminum die-cast rotor porosity on the efficiency of induction machines," *IEEE Trans. Magn.*, vol. 54, no. 11, Nov. 2018, Art. no. 8104905.
- [49] H.-W. Yang, D. H. Kang, S.-G. Kang, D. Jang, S.-W. Jung, and S.-Y. Jung, "Analysis of skewing method considering 3-D electromagnetic force," in *Proc. IEEE 20th Biennial Conf. Electromagn. Field Comput.*, 2022, pp. 1–2.
- [50] Mitsubishi Electric Corp., H. Kometani et al., "Permanent magnet rotating electric machine," JP Patent (JP4089527B2), 2008.
- [51] M. Thiele, "Analysis of cogging torque due to manufacturing variations in fractional pitch permanent magnet synchronous machine," Ph.D. dissertation, Charles Darwin Univ., Casuarina, NT, Australia, 2013.
- [52] R. Li et al., "A novel modular stator fractional pole-pair permanent-magnet Vernier machine with low torque ripple for servo applications," *IEEE Trans. Magn.*, vol. 57, no. 2, Feb. 2021, Art. no. 8102406.
- [53] G. Bramerdorfer, E. Marth, and G. Goldbeck, "Cogging torque sensitivity considering imperfect magnet positioning for permanent magnet machines of different slot and pole count," *CES Trans. Elect. Mach. Syst.*, vol. 4, no. 3, pp. 243–251, Sep. 2020.
- [54] S. Nian, L. Zhu, X. Luo, and Z. Huang, "Analytical methods for optimal rotor step-skewing to minimize cogging torque in permanent magnet motors," in *Proc. 22nd Int. Conf. Elect. Mach. Syst.*, China, 2019, pp. 1–5.
- [55] S. Zhang and S. Guo, "An analytical method for electromagnetic performance calculation in surface-mounted permanent-magnet machines with skewing," in *Proc. 21st Int. Conf. Elect. Mach. Syst.*, Jeju, South Korea, 2018, pp. 2697–2701.
- [56] C. Ma, J. Li, N. Zhang, F. Bu, and Z. Yang, "Open-circuit radial stray magnetic flux density based noninvasive diagnosis for mixed eccentricity parameters of interior permanent magnet synchronous motors in electric vehicles," *IEEE Trans. Ind. Electron.*, vol. 70, no. 2, pp. 1983–1992, Feb. 2023.
- [57] S.-H. Park, J.-W. Chin, K.-S. Cha, J.-Y. Ryu, and M.-S. Lim, "Investigation of AC copper loss considering effect of field and armature excitation on IPMSM With hairpin winding," *IEEE Trans. Ind. Electron.*, vol. 70, no. 12, pp. 12102–12112, Dec. 2023.
- [58] R. Tsunata, M. Takemoto, S. Ogasawara, and K. Orikawa, "Variable flux memory motor employing double-layer delta-type PM arrangement and large flux barrier for traction applications," *IEEE Trans. Ind. Appl.*, vol. 57, no. 4, pp. 3545–3561, Jul./Aug. 2021.
- [59] M. Aydin, Y. Demir, E. Yolacan, M. Gulec, and A. M. El-Refai, "Design and validation of an unconventional 39-slot PM synchronous motor with asymmetric and unbalanced AC windings," *IEEE J. Emerg. Sel. Topics Power Electron.*, vol. 10, no. 2, pp. 1733–1744, Apr. 2022.
- [60] K. J. Binns, A. A. K. Hameed, and F. B. Chaaban, "A canned solid rotor permanent magnet machine with skewed-radial neodymium-iron-boron magnets," in *Proc. 4th Int. Conf. Elect. Mach. Drives Conf.*, London, U.K., 1989, pp. 57–60.
- [61] R. Tsunata, M. Takemoto, J. Imai, T. Saito, and T. Ueno, "Comparison of thermal characteristics in various aspect ratios for radial-flux and axial-flux permanent magnet machines," *IEEE Trans. Ind. Appl.*, vol. 59, no. 3, pp. 3353–3367, May/June 2023.
- [62] B. Zoń and T. Węgiel, "Analysis of cogging torque reduction method effectiveness on the example of a surface mounted permanent magnet synchronous motor model," in *Proc. Int. Symp. Elect. Mach.*, Andrychów, Poland, 2018, pp. 1–5.
- [63] K.-Y. Hwang, H. Lin, S.-H. Rhyu, and B.-I. Kwon, "A study on the novel coefficient modeling for a skewed permanent magnet and overhang structure for optimal design of brushless DC motor," *IEEE Trans. Magn.*, vol. 48, no. 5, pp. 1918–1923, May 2012.
- [64] C. H. Kang, K. J. Kang, J. Y. Song, Y. J. Cho, and G. H. Jang, "Axial unbalanced magnetic force in a permanent magnet motor due to a skewed magnet and rotor eccentricities," *IEEE Trans. Magn.*, vol. 53, no. 11, Nov. 2017, Art. no. 8210505.
- [65] S. Urbaneek et al., "Design and experimental investigation of an additively manufactured PMSM rotor," in *Proc. IEEE Int. Elect. Mach. Drives Conf.*, Hartford, CT, USA, 2021, pp. 1–6.
- [66] H. Ohguchi, S. Imamori, K. Yamazaki, H. Yui, and M. Shuto, "Loss analysis of permanent-magnet synchronous machines considering in-plane eddy current in electrical steel sheets," in *Proc. Int. Power Electron. Conf.*, Niigata, Japan, 2018, pp. 699–703.
- [67] M.-M. Koo, J.-Y. Choi, K. Hong, and K. Lee, "Comparative analysis of eddy-current loss in permanent magnet synchronous machine considering PM shape and skew effect using 3-D FEA," *IEEE Trans. Magn.*, vol. 51, no. 11, Nov. 2015, Art. no. 6301104.
- [68] Z. Han, J. Liu, C. Gong, and J. Lu, "Influence mechanism on vibration and noise of PMSM for different structures of skewed stator," in *Proc. 20th Int. Conf. Elect. Mach. Syst.*, Sydney, NSW, Australia, 2017, pp. 1–5.
- [69] A. Looser, T. Baumgartner, J. W. Kolar, and C. Zwyssig, "Analysis and measurement of three-dimensional torque and forces for slotless permanent-magnet motors," *IEEE Trans. Ind. Appl.*, vol. 48, no. 4, pp. 1258–1266, Jul./Aug. 2012.
- [70] O. Ocaik and M. Aydin, "An innovative semi-FEA based, variable magnet-step-skew to minimize cogging torque and torque pulsations in permanent magnet synchronous motors," *IEEE Access*, vol. 8, pp. 210775–210783, 2020.
- [71] W. Chen, J. Ma, G. Wu, and Y. Fang, "Torque ripple reduction of a salient-pole permanent magnet synchronous machine with an advanced step-skewed rotor design," *IEEE Access*, vol. 8, pp. 118989–118999, 2020.
- [72] J. Zhao, J. Wang, L. Zhou, W. Huang, Y. Ma, and Z. Zhang, "Cogging torque reduction by stepped slot-opening shift for interior permanent magnet motors," in *Proc. 22nd Int. Conf. Elect. Mach. Syst.*, China, 2019, pp. 1–4.
- [73] Y. Zhou, J. Ji, W. Zhao, S. Zhu, and H. Liu, "Modulated vibration reduction design for integral-slot interior permanent magnet synchronous machines," *IEEE Trans. Ind. Electron.*, vol. 69, no. 12, pp. 12249–12260, Dec. 2022.
- [74] J. W. Jiang et al., "Rotor skew pattern design and optimization for cogging torque reduction," *IET Elect. Syst. Transp.*, vol. 6, no. 2, pp. 126–135, 2016.
- [75] S. Wang and H. Li, "Effects of rotor skewing on the vibration of permanent magnet synchronous motors with elastic-plastic stator," *IEEE Trans. Energy Convers.*, vol. 37, no. 1, pp. 87–96, Mar. 2022.
- [76] A. B. Letelier, D. A. Gonzalez, J. A. Tapia, R. Wallace, and M. A. Valenzuela, "Cogging torque reduction in an axial flux PM machine via stator slot displacement and skewing," *IEEE Trans. Ind. Appl.*, vol. 43, no. 3, pp. 685–693, May/June 2007.

- [77] P. Srihumpun et al., "Design optimization and comparative study of skewed Halbach-array magnets TORUS axial-flux permanent magnet motors for electric vehicles," *IEEE Access*, vol. 12, pp. 99912–99920, 2024.
- [78] R. Tsunata, M. Takemoto, J. Imai, T. Saito, and T. Ueno, "Superior efficiency under PWM harmonic current in an axial-flux PM machine for HEV/EV traction: Comparison with a radial-flux PM machine," *IEEE Trans. Ind. Appl.*, vol. 60, no. 5, pp. 6736–6751, Sep./Oct. 2024.
- [79] C. Peng, D. Wang, B. Wang, J. Li, C. Wang, and X. Wang, "Different rotor segmented approaches for electromagnetic vibration and acoustic noise mitigation in permanent magnet drive motor: A comparative study," *IEEE Trans. Ind. Electron.*, vol. 71, no. 2, pp. 1223–1233, Feb. 2024.
- [80] W. Ren, Q. Xu, Q. Li, and L. Chen, "Reducing cogging torque and suppressing torque ripple in PMSynRM for EV/HEV applications," in *Proc. IEEE ITC Asia-Pacific*, Beijing, China, 2014, pp. 1–6.
- [81] S. Roggia, G. Roggia, C. Francesco, and M. Galea, "Rotor configuration comparison for the design of a PM conical machine," in *Proc. IEEE Energy Convers. Congr. Expo.*, Baltimore, MD, USA, 2019, pp. 3976–3982.
- [82] P. Liang, D. Zhang, C. Liu, and X. Gu, "A review of conical rotor motors," in *Proc. IEEE 7th Int. Elect. Energy Conf.*, Harbin, China, 2024, pp. 1101–1106.
- [83] P. Lazari, B. Sen, J. Wang, and X. Chen, "Accurate d - q axis modeling of synchronous machines with skew accounting for saturation," *IEEE Trans. Magn.*, vol. 50, no. 11, Nov. 2014, Art. no. 8105704.
- [84] Y. An et al., "Calculation model of armature reaction magnetic field of interior permanent magnet synchronous motor with segmented skewed poles," *IEEE Trans. Energy Convers.*, vol. 37, no. 2, pp. 1115–1123, Jun. 2022.
- [85] Y.-J. Won et al., "Transfer learning-based design method for cogging torque reduction in PMSM with step-skew considering 3-D leakage flux," *IEEE Trans. Magn.*, vol. 59, no. 11, Nov. 2023, Art. no. 8204905.
- [86] J. Asama, Y. Yamamoto, T. Oiwa, and A. Chiba, "Optimal winding arrangement of a surface-mounted permanent magnet motor for torque ripple reduction," in *Proc. IEEE Energy Convers. Congr. Expo.*, Milwaukee, WI, USA, 2016, pp. 1–7.
- [87] P. Lazari, J. Wang, and B. Sen, "3-D effects of rotor step-skews in permanent magnet-assisted synchronous reluctance machines," *IEEE Trans. Magn.*, vol. 51, no. 11, Nov. 2015, Art. no. 8112704.
- [88] K. Nemoto et al., "Rotating electric machine," EP1684400B1, Jul. 2005. [Online]. Available: <https://patents.google.com/patent/EP1684400B1/ja>
- [89] W. Yunhong et al., "Multiphase skewed slot shift extremely-low vibration noise permanent magnet motor," CN11162613A, May 2020. [Online]. Available: <https://patents.google.com/patent/CN11162613A/en>
- [90] F. Liang et al., "Permanent magnet machine with different pole arc angles," US9035522B2, May 2015. [Online]. Available: <https://patents.google.com/patent/US9035522B2/en?q=US9035522>
- [91] N. Takahashi et al., "Permanent magnet electric motor," US20110309706A1, Feb. 2014. [Online]. Available: <https://patents.google.com/patent/US20110309706A1/en?q=US20110309706A1>
- [92] T. Ueda, "Motor," US9966809B2, Jan. 2016. [Online]. Available: <https://patents.google.com/patent/US9966809B2/en?q=US9966809>
- [93] N. Takahashi et al., "Rotor for rotating electrical machine," US8362668B2, Dec. 2010. [Online]. Available: <https://patents.google.com/patent/US8362668B2/en?q=US8362668>
- [94] M. Nakano et al., "Permanent magnet type motor for electric power steering," JP6124999B2, May 2017. [Online]. Available: <https://patents.google.com/patent/JP6124999B2/en?q=JP6124999B2>
- [95] T. Tanaka et al., "Embedded permanent magnet rotary electric machine," US9705366B2, Jul. 2017. [Online]. Available: <https://patents.google.com/patent/US9705366B2/en?q=US9705366>
- [96] K. Tomohara et al., "Split core for stator of rotary motor, motor stator thereof, and permanent magnet synchronous motor," JP4949271B2, Jun. 2012. [Online]. Available: <https://patents.google.com/patent/JP4949271B2/en?q=JP4949271B2>
- [97] K. Byung-kyu et al., "Method for making integrated stator, brushless direct current motor of radial core type having a structure of double rotors and method for making the same using the method," KR100663641B1, Jan. 2007. [Online]. Available: <https://patents.google.com/patent/KR100663641B1/en?q=KR100663641B1>
- [98] D. J. Patterson et al., "Permanent magnet motors and methods of assembling the same," US20130057105A1, Jan. 2007. [Online]. Available: <https://patents.google.com/patent/US20130057105A1/en?q=US20130057105A1>
- [99] R. Obata, "Systematic Surver on stamping tooling for motor core," vol. 11, Mar. 2018. [Online]. Available: <https://sts.kahaku.go.jp/diversity/document/system/pdf/109.pdf>
- [100] D. H. Park et al., "Experimental study on mixed-model production of stator and rotor using motor core laminated stamping die technology for attaching and detaching cam," *Trans. Mater. Process.*, vol. 26, no. 4, pp. 240–245, 2017.
- [101] N. Aramaki et al., "Motor, rotary electric machine and its stator, and method for manufacturing the stator," WO/2006/120975, Nov. 2006. [Online]. Available: <https://patentimages.storage.googleapis.com/43/6a/75/72c6f3ecde3d22/WO2006120975A1.pdf>



REN TSUNATA (Member, IEEE) was born in Miyagi Prefecture, Japan, in 1992. He received the B.S., M.S., and Ph.D. degrees in electrical engineering from Hokkaido University, Hokkaido, Japan, in 2015, 2017, and 2021, respectively.

He was with Toyota Motor Corporation, Aichi, Japan, during 2017–2018. In 2021, he joined Okayama University, Okayama, Japan, as a Research Fellow. He became an Assistant Professor with the Graduate School of Natural Science and Technology, Okayama University, in 2022 and has

been a Research Associate Professor since 2023. His research interests include permanent magnet synchronous machines, variable flux motors, and axial flux machines.

Dr. Tsunata is a member of the Institute of Electrical Engineers of Japan (IEEJ) and The Japan Society of Applied Electromagnetics and Machines (JSAEM). He was a recipient of four IEEJ Excellent Presentation Awards in 2017, 2020, 2022, and 2023, and the Incentive Award from JSAEM in 2020.



MASATSUGU TAKEMOTO (Member, IEEE) was born in Tokyo, Japan, in 1972. He received the B.S. and M.S. degrees in electrical engineering from the Tokyo University of Science, Noda, Japan, in 1997 and 1999, respectively, and the Ph.D. degree in electrical engineering from the Tokyo Institute of Technology, Tokyo, Japan, in 2005.

In 1999, he joined the Tokyo Institute of Technology as a Research Associate in the Department of Electrical Engineering. In 2004, he joined the Musashi Institute of Technology, Tokyo, as a

Research Associate in the Department of Mechanical Systems Engineering, where he became a Lecturer in 2005. In 2008, he joined Hokkaido University as an Associate Professor in the Graduate School of Information Science and Technology. Since 2020, he has been with Okayama University, Okayama, Japan, where he is a Professor with the Graduate School of Natural Science and Technology. He is involved in research on permanent magnet synchronous motors, axial gap motors, rare-earth-free motors, bearingless motors, and magnetic bearings.

Dr. Takemoto is a member of the Institute of Electrical Engineers of Japan (IEEJ). He was a recipient of the Nagamori Award from the Nagamori Foundation in 2017, the IEEJ Transaction Paper Award in 2005, the Prize Paper Awards from the Electric Machines Committee of the IEEE Industry Applications Society in 2011 and 2019, and the Prize Paper Award from the Electrical Machines Technical Committee of the IEEE Industrial Electronics Society in 2018. He has served as Secretary, Vice-Chair, and Chair of the IEEE IAS Japan chapter in 2008–2009, 2010–2011, and 2012–2013, respectively.